By acceptance of this article, the publisher or recipient acknowledges the U.S. Government's right to retain a nonexclusive, royalty-free license in and to any copyright covering the article.

CONF-801011--37

MASTER

ELECTRON DESIGN AND PERFORMANCE OF THE ORNL POSITIVE ION SOURCES*

J. H. Whealton, W. L. Gardner, H. H. Haselton, M. M. Menon, P. M. Ryan, J. L. Schechter, W. L. Stirling, C. C. Tsai, W. K. Dagenhart, N. S. Ponte, G. C. Barber, R. W. McGaffey, R. E. Wright

Abstract

The neutral beam development group at ORNL has designed, constructed, and shipped four 70-kV, 100-A sources to PPPL to be used for neutral beam heating of the confined plasma on the PDX tokamak. These sources have higher current capability than scaled-down sources, and they are required to run for 0.5 s as opposed to the 0.3-s requirement for PLT and ISX-B sources. Due to an innovative electrode design, these higher power sources met these requirements and achieved a higher transmission efficiency – 76% of the total input power on target vs 60% for the original ISX-B and modified PLT sources or 40% for the original PLT sources. As a consequence, a power of 2 MW of neutrals to the torus target was achieved; this is a record for measured neutral power and exceeds that of any other power source expected to be used on such advanced tokamaks as TFTR and D-III. A theoretical consideration of the relevant Poisson-Vlasov equations for ions extracted from a plasma was used to optimize the ion optics. Using the same electrode design with a tetrode accelerating structure and a new, indirectly heated cathode, repeatable long pulse, high energy conditions of 70 kV, 7 A, 8 s and 90 kV, 9 A, 5 s were achieved. Grid deformation calculations and Monte Carlo beam line gas deposition algorithms will be discussed. A direct-magnetic-electron-blocking, direct-recovery device is described, and theoretical considerations of it are discussed.

With a 40-kV, 60-A, 0.1-s source (which we designed and developed for PLT[1-18] and ISX-B[14,19-22]) as a starting point, we contracted to develop a 50-kV, 100-A, 0.5-s source for PDX and ISX-B. The scaleup in voltage and current was, to those familiar with the state of the art, a relatively predictable design,[23-33] but the increase in pulse length was much more demanding. It required, first, careful cathode design[7,34-37] and cooling design,[7,15,38-43] but even with these, the requirements were not certain to be met unless an improvement in ion optics could be incorporated into the design. Such an improvement was subject to many constraints, the principal ones being electrode transparency, electrode durability, ease of fabrication, and insensitivity to plasma imperfection. We determined that copper electrodes were adequate and decided to use circular instead of slot apertures. We further decided to use a hollow cathode electron feed source with bucket-field plasma confinement, otherwise known as the duoPIGatron,[1-4,5,12,17,23,24,44-57] as opposed to magnetic-field-free sources.

The duoPIGatron ion source was chosen because of its record high proton yield,[2-4,8,10,17,19-22,27-29,31,32,58-60] as compared to any other intense ion source[47-49,61-75] intended for neutral beam heating. The record high proton yield has been claimed[76] (and this is as yet unrefuted) to result from the separate regions of ionization and dissociation that allow more control of the proton fraction. This control is harder to achieve in a source plasma with a more uniform distribution of cathodes. The reliability, electrical efficiency, and prolific plasma production of this type source were central to its selection.

We once again decided to use circular apertures instead of slot apertures. Our original decision to use circular apertures on ORMAK, PLT, and ISX-B sources was based on prior measurements[77] that indicated inferior optical quality beams with slot apertures. We now know that the experimental evidence was inconclusive because the slot ends were not a negligible fraction of the aperture area, the source was relatively noisy,[50] and no special care was taken to shape either the slot or the circular aperture. Recent, relatively unambiguous published results[78] show that, even for endless slots, the ion beam divergence is much more critically dependent upon imperfections in the

*Research sponsored by the Office of Fusion Energy, U.S. Department of Energy, under contract W-7405-eng-26 with the Union Carbide Corporation.

DISCLAIMER

source plasma (e.g., density fluctuations, spatial variations) than it is with cylinders. In addition, for electrodes that are not carefully shaped, optimum slot aperture optics is inferior to circular aperture optics. Slot optics will rival circular optics only if the electrodes are carefully shaped and tailored for optimum conditions. Even for these conditions, however, circular aperture electrodes offer the same or better quality optics, and they are, at the same time, less sensitive to deviation from idealistic source plasma conditions. In addition, they produce far better optics for volume-produced secondary ions in the important region just outside the sheath. This latter feature results from the fact that, for the same electrode shape, slot geometry systems have higher radial fields at the optimum beam perveance than circular-shaped apertures. These considerations that favor circular optics leave open the question of the deleterious effects of the slot ends on the beam. Slot beam generators assume that the end effects are negligible to the extent that the width of the slot is less than the length of the slot. This assumption has not yet been established or refuted, but an effort is under way to conclusively delineate the slot end effect with an algorithm that can be solved using the 3-D Poisson-Vlasov equations.[79-82]

Because of such ambiguous evidence on end effects and our concern about the possibility of an imperfect source plasma, the designers at this institution chose to use circular apertures. It is only fair to say that if (1) the source plasma were to achieve a sufficient state of perfection, (2) the end effects could be made negligible, and (3) the number of volume-produced secondaries were meager, then slots would be a superior choice. Under these conditions, the transparency of the slot electrodes would potentially be higher, allowing better use of the source plasma, and the cooling and other fabricational engineering would be easier. These were the most important and the most difficult decisions to be made in choosing a design for the PDX and ISX-B ion source. The electrode shape utilized differed from the shapes used on previous sources or in previous beamlet optics studies, and it was chosen solely on the basis of the results of a theoretical consideration of the 2-D Poisson-Vlasov equation,[83-94] which had been, in all previous cases, a reliable predictor[51,53,95-100] of subsequent experimental outcome and a substantiator of prior experimental outcome.[3,101-111] The next section will describe some of the features and results of this algorithm.

Constrained by well-posed boundary conditions, we attempted to solve the Poisson-Vlasov equation:

$$\nabla^2\phi = e^{-\phi} - \int f\, dv \qquad (1)$$

and

$$(v \cdot \nabla - \nabla\phi \cdot \nabla_v)f = 0 , \qquad (2)$$

where ϕ, v, and f are the potential, the ion velocity, and the ion velocity distribution function, respectively. The techniques that we used to solve these equations are described in the literature.[83-94] The important points are that the bottleneck preventing a reasonable solution is the exponential term in Eq. (1) and that utilization of an implicit scheme for dealing with it yielded rapid convergence instead of nonsensical results. Figures 1 and 2 show the progress that has been made in the solution of Eq. (1), and Fig. 3 shows the progress that has been made in an expeditious solution of Eq. (2). A central feature of the algorithm is that the full sheath region is part of the solution, not part of the input data. (In order to use it as input data, an unreasonable assumption must be made.) A possible solution for the sheath region is shown in Fig. 4. Methods of reducing ion beamlet divergence in intense neutral beam generators include shaping the plasma electrode in the hope of diminishing, or even eliminating, aberrations caused by this electrode.[63,68-70,77,101,112-130] An extreme form of such shaping resembles a shape examined by Pierce that eliminates aberrations for electrodes emitted from a cathode in the absence of charge-compensating ions. This form has been also utilized for ion beams formed by extraction from a plasma, where a sheath develops and replaces the cathode. Three disadvantages of such a device are as follows: (1) the sensitivity of the ion optics to plasma density variation is relatively large;[50] (2) the geometrical transmission of a multiaperture electrode, due to its beveled edges, is relatively small; and (3) the optimum perveance for minimum beam divergence is relatively small since the sheath will form on the plasma side of the electrode.

Most compromise attempts to ameliorate the situation involve reducing the aberration fields. For the PDX source, the attempt is to consider a shape that does not try to reduce aberrations but merely puts them in a "closet" where the ions cannot get at them.

The class of electrode shapes we will consider is shown in Fig. 5. Three parameters will be varied — the source plasma density and dimensions b and c in Fig. 5. A blowup of Fig. 5, showing the details of an optimization of these parameters for minimum beam divergence, is shown in Fig. 4. Principal noteworthy features of this optimized situation are that the sheath forms near the axial position of the notch and that the aberrations are in a corner where ions do not penetrate.

The variation in ion optics with axial position of the notch c was considered. Three illustrative positions are shown in Figs. 4, 6, and 7 at optimized perveance. In Fig. 4, the notch is seen to be in an optimum position where the aberrations are sufficiently closeted and

the beam excluded. However, in Fig. 6 the beam is not excluded, and in Fig. 7 the aberrations are not closeted. These last two situations produce lower quality ion beams even at optimum perveance. A quantitative display of the effect of notch position on ion optics at optimum perveance is shown in Fig. 8, where an optimum notch position c/d is shown to exist.

The radial position of the notch b/a was also varied. Four illustrative positions are shown in Figs. 4 and 9-11. In Figs. 4 and 10 the aberrations are sufficiently closeted and the beam excluded. However, in Fig. 9 the beam is not excluded, and in Fig. 11, where b = ∞, the aberrations are not closeted. A quantitative display of the effect of notch depth on ion optics at optimum perveance is shown in Fig. 12, where an optimum notch depth b/a is shown to exist.

In conclusion, we note that while the optimum beam divergence is not as low for a triangular-shaped electrode in cylindrical geometry, it is smaller than the divergence for a triangular-shaped electrode in slot geometry and yields a higher optimum perveance than either for the same hole size and gap. For a multiaperture system the notch also has a higher geometric transparency than a cylindrical Pierce electrode system; however, the transparency is not as high as that of cylinder bore apertures of similar web width.

A multiaperture triode[1,3,47,49] ion accelerator was fitted to a test stand with calorimetric measurements on a downstream target. Various electrode shapes and biases were considered with regard to overall power transmission efficiency to the target, which subtends an angle of 2° at a distance of 4.5 m from the source at its focal point. Four types of electrode shapes[21,101] were considered, as is shown in Fig. 13. Type D was considered from favorable optics predictions[98] using a fast, convergent,[86,89,93] and reliable[50,51,78,95,96,99,101,103,109] 2-D algorithm. Shape C was examined on previous injectors used on the ISX-B tokamaks.[21,101] In addition, a small preacceleration potential was examined in accordance with previous theoretical predictions[95,96] and experimental findings.[51] The results, shown in Fig. 11, indicate that type D with ~50-V preacceleration potential yields the highest transmission on target (70% of the input I × V power); otherwise, type D without preacceleration potential yields 68% of the input power. In addition, the performance of the ion source used in the PLT injectors[3] is shown.

The power deposition on the other parts of the beam line (see Fig. 14) is shown in Figs. 15, 16, and 17 for sources 1, 2, and 3, respectively. The beam profile at the focal point for these sources is shown in Figs. 18-20, respectively. Such profiles are the traditional method of measuring beam divergence, but they have been repeatedly shown to give little insight as to power transmission or beam wings. This fact is just being realized now for the TFTR beams. On PDX source 4, on which complete documentation is not yet ready, power transmission of 76% of I × V on the target was achieved repeatedly.

A principal diagnostic enabling us to immediately get to the core of any particular source problem is the pinhole camera.[131,132] Although we have been touting this diagnostic for three years, we remain the only parties to utilize this extremely revealing diagnostic.

For the purposes of this discussion, it will suffice to say that the intensity of each beamlet burn mark is proportional to the intensity with which that beamlet hits the pinhole. Since the center pattern of the accompanying pinhole array picture is at the center of the target and since the target is presumed to be at the focal length, it is expected that each beamlet contributes equally to this pattern and that this contribution is of maximum intensity. Any deviation of this uniform intensity may be attributable to one of three causes: (1) unintended beamlet steering, (2) anomalously high beamlet divergence (due to a local perveance mismatch), or (3) absence of source plasma (a degenerative case of cause 2). Previous results have shown that for all normal sources, the pinhole camera pattern does not noticeably depend on either perveance or plasma density. Thus, to that extent, only case 1 contributes to the inhomogeneity observed. Furthermore, the pattern has previously been shown to be independent of pulse length; thus, grid deformation due to heating effects is eliminated. Therefore, the only conceivable explanation for the inhomogeneity observed is that anomalous beam steering is significant and is caused by imperfection of the grid manufacture. The magnitude of the imperfection is of the order of 0.020 in. (effective sideways relative displacement of the holes), which causes a 1° anomalous steering for a gap of 0.300 in.

Assuming a Gaussian beamlet with a 1/e half-width ≈ 1.3°, one readily computes that, for a situation where the source under consideration delivers 68% of I × V on target, the source would have delivered 78% of I × V on target if the apertures had been without imperfection. The multitude of pinhole images verifies the previously known conclusion of anomalous beamlet steering and demonstrates how local and unusual the steering actually is.

Pinhole camera exposures for the four PDX sources are shown in Figs. 21-24; even with the relatively high power transmission of over 70% of the input power, the source is shown to be not without imperfection.

The proton fraction exhibited by the PDX source is higher than that of any other intense neutral beam source. An explanation for this is offered by C. C. Tsai, who claims that the phenomenon is due to the separation of the ionization region from the dissociation region, meaning that the ionization occurs

first, followed by the dissociation of the molecular species. In any event, the excitement and curiosity caused by the preliminary measurements spurred other measurements, with the result that the measurement of the proton fraction of the ORNL sources has become the most solidly verified measurement of its type. It is measured by three different techniques at two different laboratories. Figures 25-27 show the mass spectrum of the residual ion beam after neutralization. The presence of an abundant quantity of protons clearly shows the success of our source.

Electrode loading due to secondaries has not gone unnoticed, and data relating to this are shown in Figs. 28-32. Figure 28 shows the pressure variation of the number 1 electrode loading. There are four modes by which the plasma electrode may receive such loading: (1) the source plasma ions and electrons may bombard it in a manner virtually independent of neutral density; (2) the primary ion beam may in part impinge upon the subsequent electrodes at a lower potential, causing the emanation of electrons, a fraction of which may intercept the plasma electrode again in a fashion independent of gas pressure; (3) secondaries produced in the acceleration region may impinge with high probability on the subsequent electrodes, producing backstreaming electrons in a manner proportional to the gas pressure; or (4) positive ions from the neutralizer may intercept the next-to-last electrode (at minimum potential), again causing the emanation of electrons, some of which will go down the accelerating column. The first mode should cause loading proportional to the source plasma density; the second mode should be dependent on beam optics or electrode deformation; the third mode should be proportional to gas pressure (it is called a volume secondary process); and the fourth mode should be proportional to the neutralizer plasma density, which should be related to the primary beam processes and, to some extent, the gas pressure. Therefore, Fig. 28, which shows the number 1 loading as a function of gas pressure, shows that in the zero pressure limit, the loading is two-thirds of the loading at 5 m-torr. Thus, mode 3 can contribute no more than 30%, since mode 4 can also be pressure dependent. This is not to say that there is negligible volume secondary production, since the low divergence, volume-produced secondary beam is not counted. In some sense the production of volume secondaries is very difficult to avoid; however, producing low divergence secondaries is within the feasibility of electrode design. It appears from the evidence available that cylinder aperture electrodes yield much lower secondary beam divergence than slot aperture electrodes. Contributions to the electrode 1 loading due to modes 2 and 4 can be distinguished by the beam perveance dependence of the former and the decel voltage dependence of the latter. Figures 29-32 demonstrate the deposition of secondaries for three PDX sources. This shows that mode 4 is likely to be (but not unambiguously) proved to have an important effect even at the critical decel potential. A theoretical investigation of this mode of electrode loading seems warranted.

To this end we consider the simultaneous Poisson-Vlasov system:[133]

$$\left.\begin{aligned} \nabla^2\phi &= e^{-\phi} - \int f\, dv && (3)\\ (v\cdot\nabla - \nabla\phi\cdot\nabla_v)f &= 0 && (4)\\ (v\cdot\nabla + \nabla\phi\cdot\nabla_v)f_{se} &= 0 && (5)\end{aligned}\right\} R_1$$

and

$$\left.\begin{aligned} \nabla^2\phi &= \exp(\phi - \phi_0) - \int f_{si}\, dv_{si} && (6)\\ (v_{si}\cdot\nabla - \nabla\phi\cdot\nabla_v)f_{si} &= 0 && (7)\end{aligned}\right\} R_2 ,$$

where the subscript se refers to secondary electrons, si refers to secondary ions from the neutralizer, and ϕ denotes the potential of the neutralizer plasma. Equations (3) and (4) are solved iteratively (as previously described[86,89,93,94]) in a region R1, as is shown in Fig. 33. Electrons are then ejected from some electrode surface, as is shown in Fig. 34, and Eq. (5) above is solved for the potentials generated by the solution to Eqs. (3) and (4). In addition, a region denoted as R2 in Fig. 33 is examined in detail (see Fig. 35). In this region Eqs. (6) and (7) above are solved iteratively (as previously described[86,89,93,94]), subject to the Dirichlet boundary, whose potential and shape are chosen from the solution in R1 to Eqs. (3) and (4) above. The decel potential in Fig. 35 is near the level critical for neutralizer plasma electron blocking. The neutralizer plasma is shown on the right-hand side of Fig. 33, where its effects on the solution to the solved equations there are justifiably ignored. In Fig. 35, the neutralizer plasma is taken to be a collisionless plasma with a Boltzmann electron distribution as indicated by the fourth equation above.

From the most elementary consideration of Eqs. (3)-(7) above, there evolve three design scenarios that will minimize the loading on electrode 1. In the first case, if the positive ions from the neutralizer (as shown in Fig. 35) could be made to hit the left-hand electrode, the results would be as follows: (1) no electrons would hit electrode 1, (2) no electrons would go down the column, and (3) no power would

be lost because of ions being drawn into the right-hand electrode in Fig. 35. This would be the best of all possible solutions (T1 ≡ trap 1) if it could be effected without undue inconvenience. Barring this veritable panacea, we can fall back on the scenario in which the ions hit the right-hand electrode in Fig. 35 while all the electrons emanating therefrom go down the decel gap (to the right in Fig. 34) instead of traversing the accel gap (to the left in Fig. 34). This leaves a minor electrical power loss caused by energizing the ions and secondary electrons to 1000 V and heating the insulted electrode. This may be a source of inconvenience due to the possible gas desorption from this electrode caused by the 1000-V ions. We will designate as T2 the scenario in which the electrons are tricked into choosing the small opening instead of the big one. An even less desirable solution involves allowing the electrons to fall down the accel column (to the left in Fig. 34) while diverting them from electrode 1 and causing them to go through the aperture into the plasma generator. We will call this T3.

First we will consider T1, in which the ions are tricked into hitting the neutralizer electrode. An obvious way to effect T1 is to use a thick electrode as the left-hand electrode in Fig. 35. Another way is to apply a precel potential[51,95,96,108] to make the electrode more negative than the neutralizer potential by an amount more than that dictated by the neutralizer electron temperature and by the net current allowed to pass through the electrode in an external circuit.

The effect of varying the last electrode thickness is illustrated in Figs. 36-38, where the thickness is increased by a factor of 3. Ions are more strongly attracted to this electrode as a result, as is shown quantitatively in Fig. 39, where T1 is increased from 45% to 75% because of the doubled thickness. After that increase, it is probably beyond the point of diminishing returns to continue to increase the electrode thickness. Ion electrode attraction due to precel is illustrated in Figs. 40-43. The more overdense the neutralizer ion beam (a condition virtually guaranteed to obtain near the critical decel potential with a finite-density neutralizer plasma), the more effective the precel is in trapping ions. In addition, the effectiveness of the precel in trapping ions is accentuated by the first remedy (making the last electrode thicker), as is illustrated in Fig. 39 by the applied curve labeled 200 V, where a 200-V precel was applied. In this case the application of a 200-V precel increased T1 from 45% to 68% for the standard thickness electrode and from 75% to 93% for the double thickness electrode. Using both, the trap T1 increases from 45% to 93%, or, to put it another way, there is an 83% reduction in the number of ions reaching the next-to-last electrode. Neither of these techniques has been tried yet.

Next we will consider T2. Figure 34 is an illustration of electron dispatchment for electrons uniformly emitted from the second electrode. As can be seen, about half the electrons fall down the accel gap, and of these over half hit electrode 1. Illustrations of a few different electrode shapes are shown in Figs. 44-56 (one is an extension of the shape shown in Fig. 34). Figures 47-50 show the electron dispatchment in other cases. Figure 44 is congruent with the PDX injector design; it seems to make no attempt to divert the electrons (80% of them falling down the accel column). The shape shown in Fig. 46 seems moderately successful in diverting the electrons (only 5% of them fall the wrong way). However, the class of electrode shapes shown in Figs. 34 and 47-50 seems to trap the electrons adequately with a design like that shown in Fig. 48. It fails to trap 3%, whereas that in Fig. 44 fails to trap 70% in the corresponding region. Combining the two trapping ploys for T1 with the electrode shape shown in Fig. 48 yields a combined reduction in electron backsliders of 99.45%; at least some of this reduction is bound to obtain, even given the realities that this calculation ignores. The tricking mechanism T3 — being more sensitive to the exact details of the calculation and to the ignored phenomena for the sake of expeditiousness and being utilized with profit only after one has already seen the deficiencies of the first two trick attempts — will not be discussed and is, at best, probably in the domain of diminishing returns.

Accelerator designs for TFTR[130] and the Culham JET[134] design neglect T1 by making the last electrode relatively thin, and they also neglect the fact that (as is implied in Figs. 37-38 and 40-43) there are unreachable areas for neutralizer ions on the inside of the next-to-last electrode, consideration of which could provide a better design for T2. Unambiguous calculations to this effect show another advantage of an algorithm that solves Eqs. (1) and (2) without recourse to the specification of sheath shape[86,89,93,94] as opposed to those needing such specification.[121,134-137] By making the next-to-last electrode thinner and more skewed, it is possible to make T2 much higher. The greatest emphasis of these designs is directed toward maximization of T3.

A closer examination of the electrode shapes shown in Figs. 47-50 seems warranted since impingement from the primary ion beam is not impossible. First, to show that the shape of the downstream electrode has no effect on primary ion optics as long as the aperture is big enough and to quantify the findings in Figs. 47-50, we offer Fig. 51; it shows that the optics is unchanged to within 3% for a change of a factor of 2.5 in downstream electrode diameter. Also, the T2 trapping mechanism appears monotomically more effective

with decreasing electrode radius in the event that there is no primary interception in the T3 scenario to prevent electrode 1 interception. Beam divergence as a function of current density is shown in Fig. 52. Also shown is the radius of the beam at electrodes 2 and 3; these are denoted by e2 and e3, respectively. Typical beam trajectories for a vastly undense case (j = 175 mA/cm^2) are shown in Fig. 53; an emittance diagram for this case is shown in Fig. 54. Corresponding illustrations are shown in Figs. 55 and 56 for the overdense case of j = 525 mA/cm^2. The window of currents without electrode interception is shown in Fig. 57, which also shows which electrode provides which boundary.

Learning from our experience with the PDX and ISX-B sources, we used a notched electrode tetrode for long pulse, high energy studies. A 10 × 25 cm tetrode, positive ion source was operated at energies in excess of 100 keV and pulse lengths up to 8 s. The first gap was 6.2 mm, and the second gap was 10 mm. A notched electrode[53,97,98] was used with further guidance from single beamlet tetrode studies.[102,138] The highest voltage at which the source was operated was 107 kV, and the extracted current density at optimum would translate to about 0.5 A/cm^2 at 120 kV. HWHM divergence angles as low as 0.5° (see Fig. 58) and power transmission efficiencies exceeding 80% in ±2° were measured by carefully partitioning the voltage (in order to maintain a high electric field ratio between the second and the first gap). Such a mode of operation is generally used at the expense of current density and source reliability. The characteristics of this source under more typical operating conditions are shown in Fig. 59. The grid loadings were less than 1.5% on each of the four grids under optimum conditions, and the electron backstreaming into the plasma generator was less than 1.5% at 80-keV beam energy.

The pulse length of the beam was extended, using conventional oxide filaments, to 1.7 s at 100 kV and 6 A, to 2 s at 90 kV and 11 A, and to 4 s at 86 kV and 10 A. This filament, however, was not successful in extending the pulse length to 5 s at 86 kV and 10 A. Long pulse operation was resumed using a specially prepared, indirectly heated cathode; pulse lengths of 8 s at 70 kV and 7 A and of 5 s at 80 kV and 8 A and 90 kV and 9 A were obtained repeatedly. Further extension of the pulse length was prevented by power dissipation problems associated with certain high voltage resistors in the circuit. Measurements of power dissipation on the grids showed no signs of deterioration of the beam up to the full 8 s (see Fig. 60).

The water-cooled grids of the ion sources can receive a thermal load of about 2% of the extracted ion beam power. It has long been a concern that this level of thermal loading may mechanically deform the grids and thus degrade the injector performance. A thermal deformation analysis of the plasma grid of the ion accelerator has been performed for the PDX injector development. By employing a 3-D finite element code,[40,41] it was found that a water-cooled copper grid with a loading of 250 W/cm^2 reaches a maximum steady-state temperature of 200°C. This yields a maximum vertical displacement of 0.25 cm and a maximum radial displacement of 0.013 cm, which could significantly degrade the beam transmission. The importance or validity of this study has not yet been established. It was suggested that a high bellows kink outside the aperture pattern and movable grid edges could reduce the grid's thermal deformation. The idea of a movable grid edge was adopted for the study of an ion source compatible with TFTR (having a 15 × 43 cm grid aperture pattern, with water cooling across the narrow dimension). The results of this study indicated that the thermal deformation would be negligible.[42]

Calculations with the Monte Carlo Simulation Code[139] were extended to simulate neutral particle transport in a fully detailed PDX beam line. The geometry faithfully renders all essential features; for example, even the individual cryopump chevrons are inserted as boundary conditions. Figure 61 shows neutral pressures and densities per particle along the beam line axis for a cosine-distributed source of particles located at the ion source grids. The pressure in the drift region is reduced by nearly a factor of 3 when a drift tube cryopump is added in the drift chamber.[140] Other calculations of pressures at actual locations of ion gauges on the existing beam line agreed within 25% with the pressures observed on the gauges.

Future positive ion sources, as envisioned at the present time, will have low electrical efficiency at high energy. Besides the economic issues associated with this, targets for the residual ion beams have yet to be designed because of the high power densities. A way around both of these problems is direct recovery of the ion beam.

All schemes proposed so far outside of this laboratory have apparently had fatal flaws. The direct-recovery scheme proposed here[141-145] has not yet proved itself a failure and is therefore being pursued both theoretically and experimentally with all allowable vigor. The experimental results have shown extensive neutralizer electron suppression (patent pending) and definite ion recovery; the latest results will be reported at the Accelerator Applications Conference in Denton, Texas, by the principal investigator. The general features of the device are shown in Figs. 62 and 63. The ions are ejected out of a neutralizer, which is at the accelerator potential below ground, and they bend in the transverse magnetic field. The ions are then

recovered if they hit any grounded surface. A device is effective if it can entice the electrons into going in the desired direction and control which surfaces the molecular ions intercept. Our device is claimed[144] to have an ion recovery efficiency of 80 ± 20%. A theoretical understanding will greatly aid in further development of this device, and, to date, with one minor exception,[146] almost no information has been presented. The following paragraph deals with this matter.

In order to give a preliminary description of the magnetic-blocking, direct-recovery device (Fig. 64), we solve the following Poisson-Vlasov equations in infinite slot geometry:

$$\nabla^2\phi = 0 \ , \qquad \{R_1\} \qquad (8a)$$

$$\nabla^2\phi = e^{-\phi} - \int f \, dv \ , \qquad \{R_2\} \qquad (8b)$$

and

$$[v \cdot \nabla + (v \times B - \nabla\phi) \cdot \nabla_v] f = 0 \ , \qquad (9)$$

where $\{R_1\}$ and $\{R_2\}$ are shown in Fig. 65 and f is the ion distribution function. The neutralizer electrons are accounted for by assuming no net charge in the neutralizer $\{R_1\}$. The exponential term in Eq. (8b) represents an equilibrium distribution of target plasma electrons.[147]

Three major results are reported here.

(1) The window of acceptance for recovery varies sharply with the boost voltage [see Figs. 66-70 of the vacuum case, where ϕ in Eq. (9) is replaced by the applied fields]. For 3% excess ion velocity (Fig. 68), 54% of the ions get recovered; 27% of the ions escape the neutralizer cell but are outside the acceptance window (i.e., they have a large transverse velocity upon slowing down); and 19% of the ions intercept the walls of the neutralizer.

(2) The existence of an equilibrium target plasma increases the ion recovery efficiency.[146] This is shown in Figs. 71-75 with a target plasma and in Fig. 68 without a target plasma; it is shown quantitatively in Fig. 76.

(3) The ion space charge for high current densities reduces recovery efficiency, as is shown qualitatively in Figs. 71-75 and quantitatively in Fig. 77.

Now we know that Eq. (8a) is a poor representation of the electron density because when the electrons go faster and the ions go slower, a surplus of ion density appears to be mitigated by the small gyroradius of the electrons; therefore, Eq. (8a) should be considered a lower bound for the electron influence on the ions. A representation yielding a more realistic degree of electron influence is the replacement of Eq. (8a) by

$$\phi(x) = \phi_o \ , \quad \nabla \times \varepsilon \ \{R_1\} \qquad (10)$$

which, along with the solution of Eqs. (8b) and (9), yields Fig. 78 for the case of Fig. 73, which was the solution to Eqs. (8a), (8b), and (9). A notable result is that the recovery efficiency is higher due to target plasma. The double sheath is thinner. As a further improvement, we are in the preliminary stages of considering a double Vlasov system:

$$\nabla^2\phi = e^{-\phi} - \int f \, dv + \int f_e \, dv_e \ , \qquad (11)$$

$$[v \cdot \nabla + (v \times B - \nabla\phi) \cdot \nabla_v] f = 0 \ , \qquad (12)$$

$$[v_e \cdot \nabla - (v_e \times B - \nabla\phi) \cdot \nabla_v] f_e = 0$$

$$\text{(weak B)} \ , \qquad (13a)$$

and

$$-\nabla\phi \cdot \nabla f_e = 0 \quad \text{(strong B)} \ , \qquad (13b)$$

where f_e is the electron distribution function and Eq. (13b) is the guiding-center approximation. A preliminary result is shown in Fig. 79. By this means [Eqs. (11)-(13b)], we can not only have an accurate result for the electron influence on the ions, but also for the first time we can examine the electron deposition and establish the stability of this device for large ion current density. A 3-D computation[79-82] is also under way.

References

1. W. L. Stirling et al., Rev. Sci. Instrum. 48, 533 (1977).
2. W. L. Stirling et al., Rev. Sci. Instrum. 50(5), 523 (1979).
3. M. M. Menon et al., J. Appl. Phys. 50(4), 2484 (1979).
4. H. P. Eubank et al., Phys. Rev. Lett. 43(4), 270 (1979).
5. W. L. Stirling et al., Bull. Am. Phys. Soc. 20, 1365 (1975).
6. H. H. Haselton et al., Bull. Am. Phys. Soc. 20, 1275 (1975).

7. H. H. Haselton et al., *Proc. 6th Symp. on Engineering Problems of Fusion Research* (1975).
8. H. H. Haselton et al., Bull. Am. Phys. Soc. 21, 1082 (1976).
9. J. Kim et al., *Proc. 2nd Annual American Nuclear Society Safety Meeting on the Technology of Controlled Nuclear Fusion* (1976).
10. H. H. Haselton et al., Bull. Am. Phys. Soc. 22, 1080 (1977).
11. W. K. Dagenhart et al., *Proc. 7th Symp. on Engineering Problems of Fusion Research* (1977).
12. C. C. Tsai et al., *Proc. 7th Symp. on Engineering Problems of Fusion Research* (1977).
13. H. H. Haselton, Trans. Am. Nucl. Soc. (1977).
14. H. H. Haselton et al., *Proc. Joint Varenna-Grenoble Int. Symp. on Heating in Toroidal Plasmas* (1978).
15. H. H. Haselton, Oak Ridge National Laboratory Report ORNL/TM-5234 (1976).
16. W. K. Dagenhart, Oak Ridge National Laboratory Report ORNL/TM-6374 (1978).
17. C. C. Tsai et al., Oak Ridge National Laboratory Report ORNL/TM-6360 (1978).
18. M. M. Menon et al., Oak Ridge National Laboratory Report ORNL/TM-6658 (1979).
19. J. Kim et al., Nucl. Fusion (1979).
20. J. Kim et al., Bull. Am. Phys. Soc. 23, 1049 (1978).
21. J. Kim, Oak Ridge National Laboratory Report ORNL/TM-6896 (1979).
22. J. Kim et al., Bull. Am. Phys. Soc. 23, 746 (1978).
23. C. C. Tsai et al., Bull. Am. Phys. Soc. 21, 1082 (1976).
24. W. L. Stirling et al., Bull Am. Phys. Soc. 22, 1083 (1977).
25. G. C. Barber et al., *Proc. 7th Symp. on Engineering Problems of Fusion Research* (1977).
26. C. C. Tsai et al., Bull. Am. Phys. Soc. 23, 748 (1978).
27. J. H. Whealton et al., *Proc. IAEA Workshop on Neutral Injectors* (1978).
28. W. L. Gardner et al., *Proc. 8th Symp. on Engineering Problems of Fusion Research* (1979).
29. M. M. Menon et al., *Proc. 8th Symp. on Engineering Problems of Fusion Research* (1979).
30. R. E. Wright et al., *Proc. 8th Symp. on Engineering Problems of Fusion Research* (1979).
31. W. L. Gardner et al., paper presented at the 21st Annual Meeting of the Division of Plasma Physics of the American Physical Society, Boston, Massachusetts, 1979.
32. W. L. Gardner et al., paper presented at the IEEE Conf. on Plasma Science, Madison, Wisconsin, 1980.
33. S. W. Schwenterly, *Proc. 7th Symp. on Engineering Problems of Fusion Research* (1977).
34. D. E. Schechter et al., Bull. Am. Phys. Soc. 23, 747 (1978).
35. C. C. Tsai et al., *Proc. IEEE Int. Conf. on Plasma Science* (1979).
36. D. E. Schechter et al., *Proc. 8th Symp. on Engineering Problems of Fusion Research* (1979).
37. J. Kim et al., paper presented at the 21st Annual Meeting of the Division of Plasma Physics of the American Physical Society, Boston, Massachusetts, 1979.
38. W. Gambill et al., Bull. Am. Phys. Soc. 21, 1030 (1976).
39. J. Kim et al., *Proc. 7th Symp. on Engineering Problems of Fusion Research* (1977).
40. D. A. Everitt et al., *Proc. 8th Symp. on Engineering Problems of Fusion Research* (1979).
41. J. A. Mayhall and C. C. Tsai, *Proc. 8th Symp. on Engineering Problems of Fusion Research* (1979).
42. McDonnel Douglas Corporation Report MDC E2204 (1980).
43. L. Bromberg, private communication, 1976.
44. G. G. Kelley et al., Nucl. Instrum. Methods 10, 263 (1961).
45. O. B. Morgan et al., Rev. Sci. Instrum. 4, 467 (1967).
46. G. G. Kelley, IEEE Trans. Nucl. Sci. 14, 29 (1967).
47. W. L. Stirling, Rev. Sci. Instrum. 43, 278 (1972).
48. G. G. Kelley et al., Nucl. Fusion 12, 169 (1972).
49. R. C. Davis et al., Rev. Sci. Instrum. 46, 576 (1975).
50. J. H. Whealton and C. C. Tsai, Rev. Sci. Instrum. 49, 495 (1978).
51. J. H. Whealton et al., Appl. Phys. Lett. 33, 278 (1978).
52. W. L. Stirling et al., Rev. Sci. Instrum. 50, 102 (1979).
53. W. L. Gardner et al., submitted to Appl. Phys. Lett.
54. C. C. Tsai et al., Bull. Am. Phys. Soc. 20, 1365 (1975).
55. H. E. Ketterer et al., Bull Am. Phys. Soc. 20, 1333 (1975).
56. W. L. Stirling et al., Bull. Am. Phys. Soc. 21, 1082 (1976).
57. P. M. Ryan et al., Bull. Am. Phys. Soc. 22, 1083 (1977).
58. J. Kim and H. H. Haselton, J. Appl. Phys. 50(6), 3802 (1979).
59. M. M. Menon, *Proc. IEEE Int. Conf. on Plasma Science* (1979).
60. J. Kim and H. H. Haselton, Oak Ridge National Laboratory Report ORNL/TM-6302 (1978).

61. O. B. Morgan, *Proc. 2nd Symp. on Ion Sources and Formation of Ion Beams* (1974).
62. L. D. Stewart et al., *Proc. 3rd Symp. on Toroidal Plasma Confinement* (1973).
63. T. Sagawara et al., Japan Atomic Energy Research Institute Report JAERI-M-7043 (1977).
64. D. Aldcroft et al., Nucl. Fusion 13, 393 (1973).
65. M. Fumelli and F. P. G. Valckx, Nucl. Instrum. Methods 135, 203 (1976).
66. J. Kim and R. C. Davis, Appl. Phys. Lett. 30, 130 (1977).
67. G. W. Hamilton et al., Plasma Phys. 10, 687 (1967).
68. K. H. Berkner et al., *Proc. 2nd Symp. on Ion Sources and Formation of Ion Beams* (1974).
69. K. W. Ehlers et al., *Proc. 9th Symp. on Fusion Technology* (1976).
70. S. M. Hibbs, *Proc. 6th Symp. on Engineering Problems of Fusion Research* (1975).
71. K. W. Ehlers et al., J. Vac. Sci. Technol. 10, 922 (1973).
72. K. H. Berkner et al., Nucl. Fusion 15, 249 (1975).
73. K. H. Berkner et al., Bull. Am. Phys. Soc. 24, 971 (1979).
74. J. F. Toaker et al., Bull. Am. Phys. Soc. 25, 974 (1980).
75. K. H. Berkner et al., *Proc. 8th Symp. on Engineering Problems of Fusion Research* (1979).
76. C. C. Tsai (Oak Ridge National Laboratory), private communication, 1978.
77. S. Matsuda et al., Bull. Am. Phys. Soc. 18, 132 (1973).
78. J. H. Whealton et al., Appl. Phys. Lett. 36, 91 (1980).
79. L. J. Drooks et al., Bull. Am. Phys. Soc. 23, 846 (1978).
80. L. J. Drooks et al., Oak Ridge National Laboratory Report ORNL/TM-6740 (1979).
81. J. W. Wooten et al., *Proc. 3rd Int. Symp. on Computer Methods for Partial Differential Equations* (1979).
82. J. W. Wooten et al., paper presented at the 21st Annual Meeting of the Division of Plasma Physics of the American Physical Society, Boston, Massachusetts, 1979.
83. E. F. Jaeger and J. C. Whitson, Bull. Am. Phys. Soc. 20, 1365 (1975).
84. E. F. Jaeger and J. C. Whitson, Oak Ridge National Laboratory Report ORNL/TM-4990 (1975).
85. J. H. Whealton et al., Bull. Am. Phys. Soc. 21, 1066 (1976).
86. J. H. Whealton et al., J. Comput. Phys. 27, 333 (1978).
87. J. C. Whitson et al., Bull. Am. Phys. Soc. 22, 1114 (1977).
88. J. H. Whealton and J. C. Whitson, Bull. Am. Phys. Soc. 23, 151 (1978).
89. J. C. Whitson et al., J. Comput. Phys. 28, 408 (1978).
90. J. H. Whealton, paper to be presented at the 6th Conf. on the Application of Acceleration in Research and Industry, November 3, 1980.
91. J. C. Whitson et al., Oak Ridge National Laboratory Report ORNL/TM-6512 (1978).
92. J. H. Whealton and J. C. Whitson, Part. Accel. 11, 14 (1980).
93. J. H. Whealton, to be published in J. Comput. Phys.
94. J. H. Whealton, to be published in Nucl. Instrum. Methods.
95. J. H. Whealton et al., J. Appl. Phys. 49, 3091 (1978).
96. J. H. Whealton and J. C. Whitson, J. Appl. Phys. 50, 3964 (1979).
97. J. H. Whealton et al., to be published in J. Appl. Phys.
98. J. H. Whealton et al., paper presented at the 21st Annual Meeting of the Division of Plasma Physics of the American Physical Society, Boston, Massachusetts, 1979.
99. J. H. Whealton, Appl. Phys. Lett. 33, 697 (1978).
100. L. R. Grisham et al., *Proc. IEEE Int. Conf. on Plasma Science* (1977).
101. L. R. Grisham et al., Rev. Sci. Instrum. 48, 1037 (1977).
102. C. N. Meixner et al., submitted to J. Appl. Phys.
103. J. Kim et al., J. Appl. Phys. 49, 517 (1978).
104. J. Kim and G. Schilling, Bull. Am. Phys. Soc. 20, 1366 (1975).
105. G. Schilling et al., Bull. Am. Phys. Soc. 21, 1065 (1976).
106. L. R. Grisham et al., Bull. Am. Phys. Soc. 21, 1065 (1976).
107. J. H. Whealton and J. Kim, Bull. Am. Phys. Soc. 22, 1114 (1977).
108. J. H. Whealton, *Proc. Annual Controlled Fusion Theory Conf.* (1977).
109. J. H. Whealton et al., Rev. Sci. Instrum. 48, 829 (1977).
110. M. M. Menon et al., Bull. Am. Phys. Soc. 23, 746 (1978).
111. J. H. Whealton et al., *Proc. IEEE Int. Conf. on Plasma Science* (1979).
112. W. S. Cooper et al., Nucl. Fusion 12, 263 (1972).
113. E. Thompson, Part. Accel. 4, 69 (1972).
114. Y. Ohara, Japan Atomic Energy Research Institute Report JAERI-Mp6813 (1966).
115. Y. Ohara et al., *Proc. 7th Symp. on Engineering Problems of Fusion Research* (1977).
116. H. R. Kaufman, Lewis Research Center Report NASA TND-585 (1961).
117. W. C. Lathem, J. Spacecr. Rockets 5, 735 (1968).
118. Y. P. Grigorev, Sov. Phys-Tech. Phys. 16, 909 (1971).
119. K. W. Ehlers et al., J. Vac. Sci. Technol. 10, 922 (1973).

120. V. M. Kulygin et al., *Proc. 2nd Symp. on Ion Sources and Formation of Ion Beams* (1974).
121. W. S. Cooper et al., *Proc. 2nd Symp. on Ion Sources and Formation of Ion Beams* (1974).
122. H. R. Kaufman, in *Advances in Electronics and Electron Physics*, ed. L. Marton (Academic Press, New York, 1974), Vol. 36.
123. T. S. Green, Rep. Prog. Phys. 37, 1287 (1974).
124. K. H. Berkner et al., Bull. Am. Phys. Soc. 21, 1136 (1976).
125. K. W. Ehlers, *Proc. IEEE Int. Conf. on Plasma Science* (1977).
126. K. H. Berkner et al., *Proc. IEEE Int. Conf. on Plasma Science* (1977).
127. T. S. Green, IEEE Trans. Nucl. Sci. *NS-23*, 918 (1976).
128. Y. Ohara et al., Jpn. J. Appl. Phys. 15, 135 (1976).
129. K. Asai et al., Jpn. J. Appl. Phys. 15, 1343 (1976).
130. K. H. Berkner et al., Bull. Am. Phys. Soc. 22, 1082 (1977); also in *Proc. 7th Symp. on Engineering Problems of Fusion Research* (1977).
131. P. M. Ryan et al., Bull. Am. Phys. Soc. 20, 1365 (1975).
132. P. M. Ryan et al., Rev. Sci. Instrum. 50, 1160 (1979).
133. J. H. Whealton et al., paper presented at the IEEE Conf. on Plasma Science (Madison, Wisconsin, 1980).
134. A. J. T. Holmes et al., *Proc. 3th Symp. on Engineering Problems of Fusion Research* (1979).
135. V. Hamsa and E. A. Richley, NASA TND-1323 (Cleveland, 1962) and NASA TND-1665 (Cleveland, 1963).
136. V. Hamsa, NASA TND-1711 (Cleveland, 1963).
137. P. T. Kirstein and J. S. Hornsby, CERN 63-16 (Geneva, 1963).
138. C. N. Meixner et al., paper presented at the 21st Annual Meeting of the Division of Plasma Physics of the American Physical Society, Boston, Massachusetts, 1979.
139. M. B. Emmett, Oak Ridge National Laboratory Report ORNL/TM-4972 (1975).
140. R. A. Lillie et al., *Proc. ANS Winter Meeting* (1979).
141. W. L. Stirling et al., Bull. Am. Phys. Soc. 23, 747 (1978).
142. J. Kim et al., *Proc. IEEE Int. Conf. on Plasma Science* (1979).
143. W. K. Dagenhart et al., *Proc. IEEE Int. Conf. on Plasma Science* (1979).
144. J. H. Whealton et al., Oak Ridge National Laboratory Report ORNL/TM-6944 (1979).
145. W. L. Stirling et al., Appl. Phys. Lett. 35, 104 (1979).
146. J. H. Whealton et al., Nucl. Instrum. Methods 154, 441 (1978).
147. J. H. Whealton et al., Bull. Am. Phys. Soc. 25, 983 (1980).

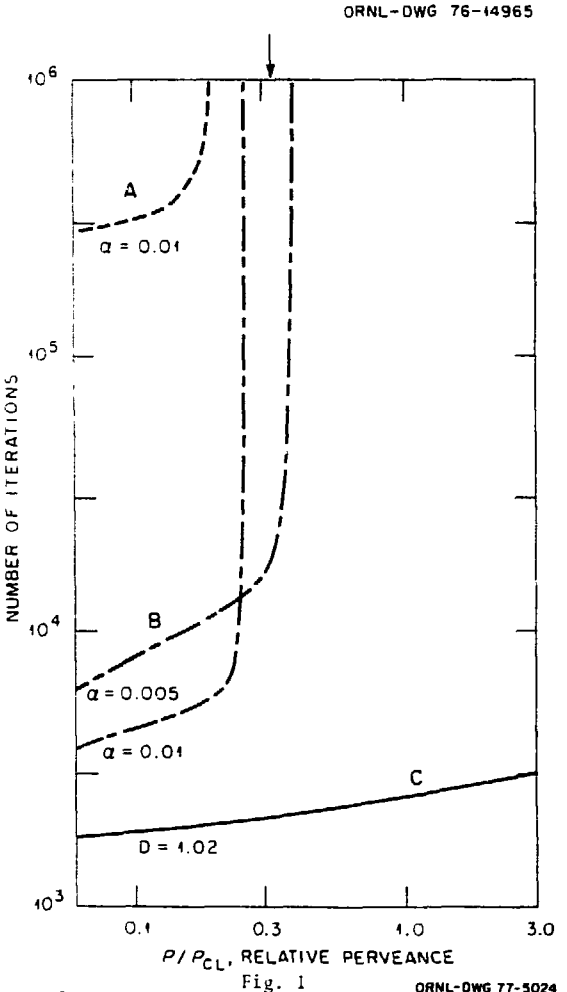

Fig. 1

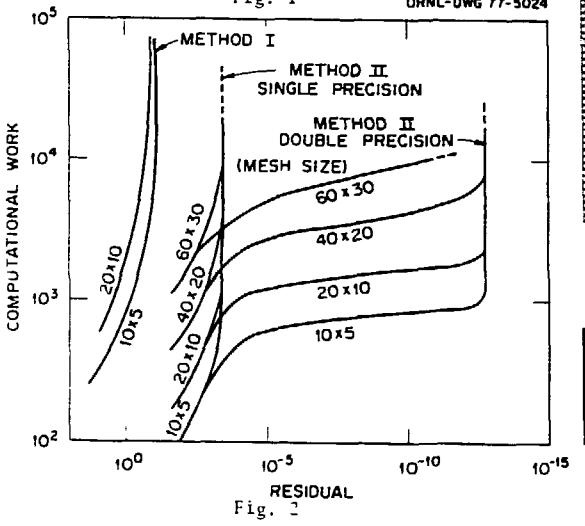

Fig. 2

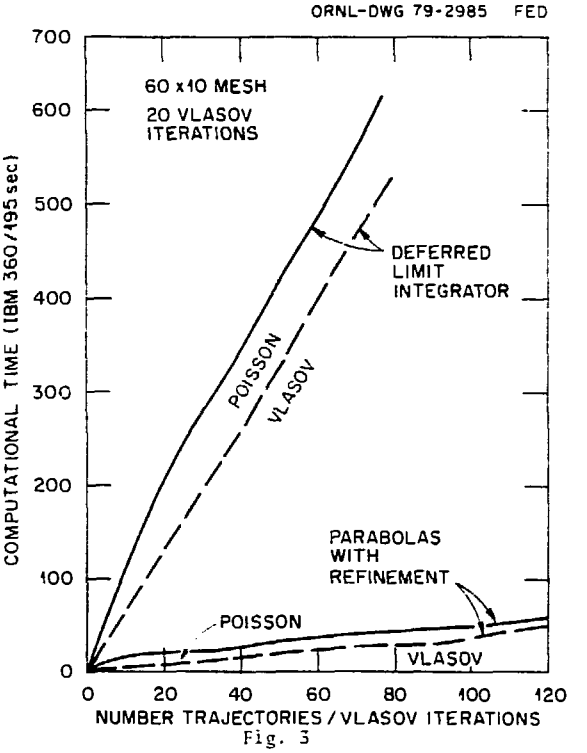

Fig. 3

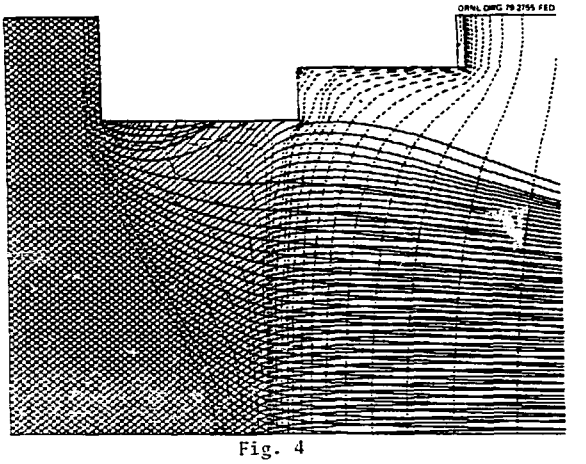

Fig. 4

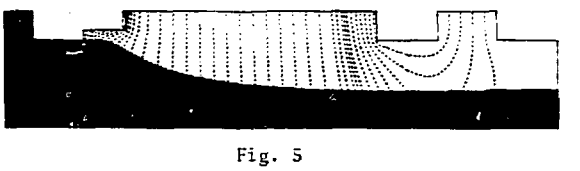

Fig. 5

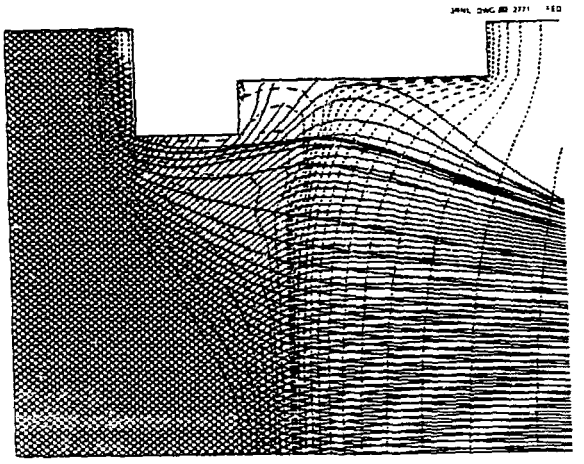

Fig. 6

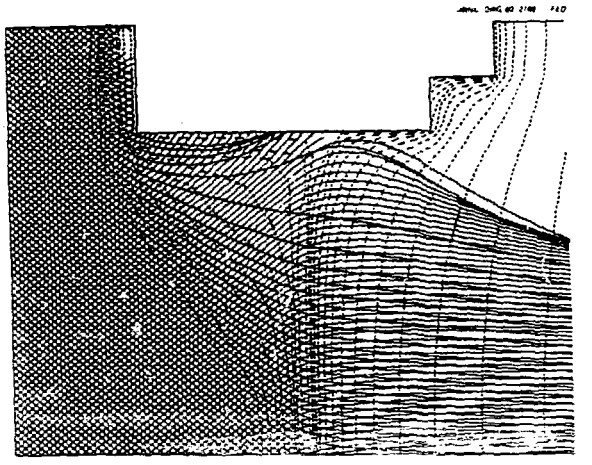

Fig. 7

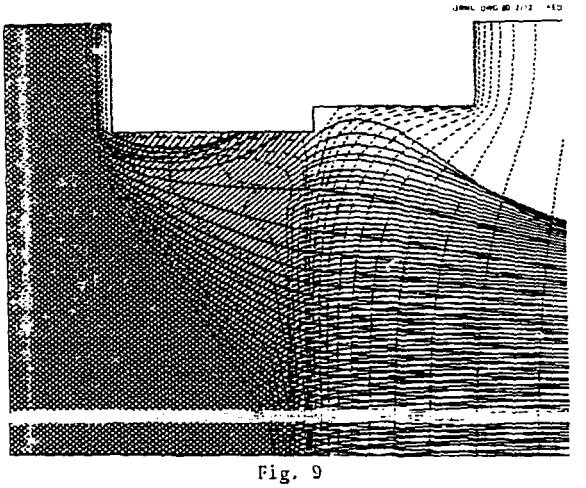

Fig. 9

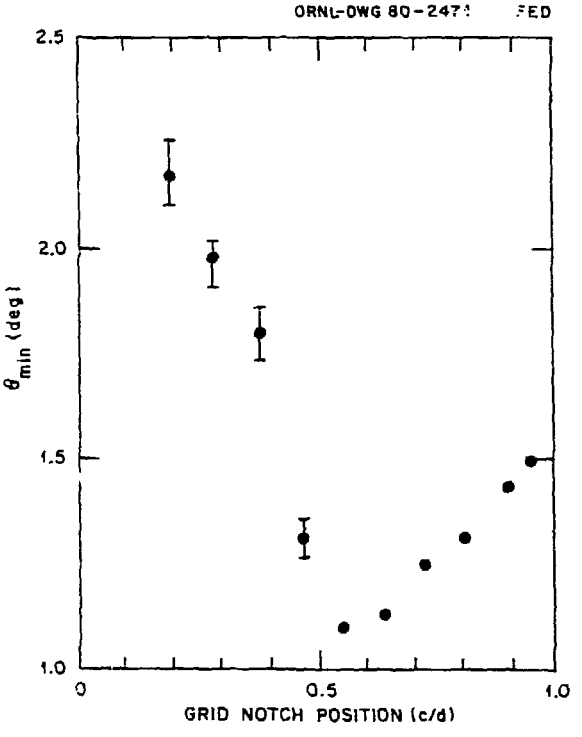

Fig. 8

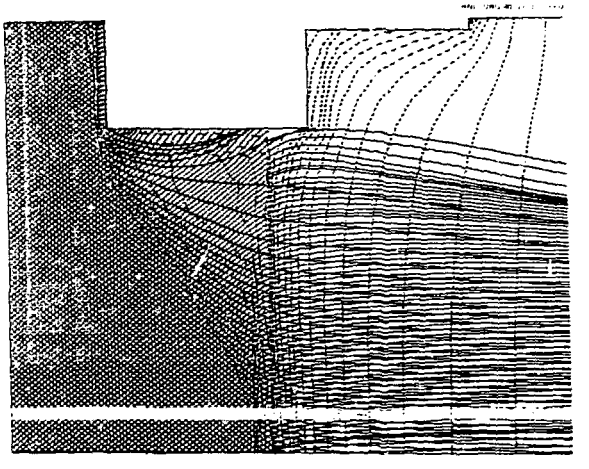

Fig. 10

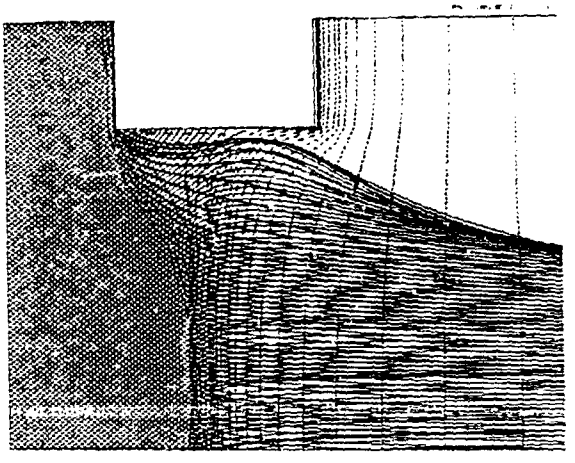

Fig. 11

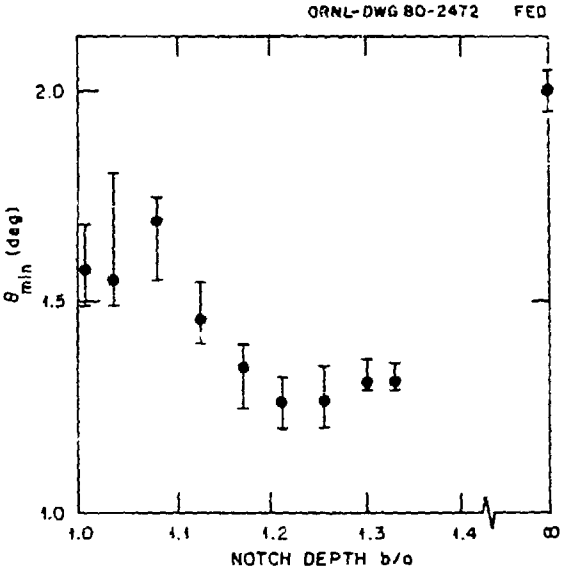

Fig. 12

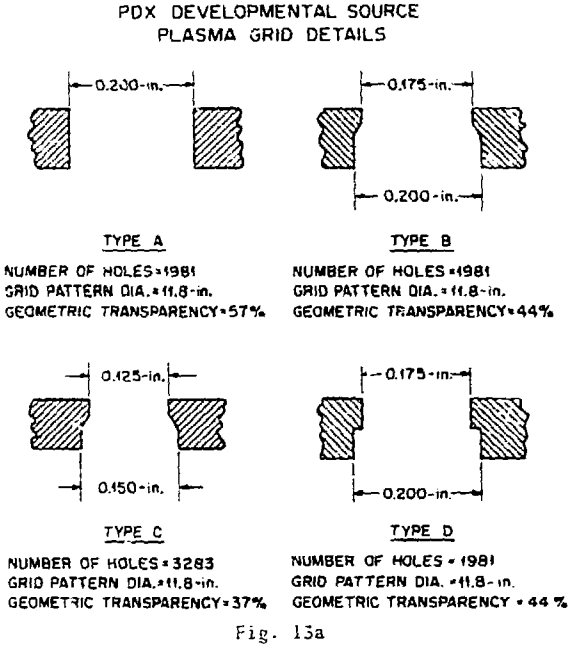

Fig. 13a

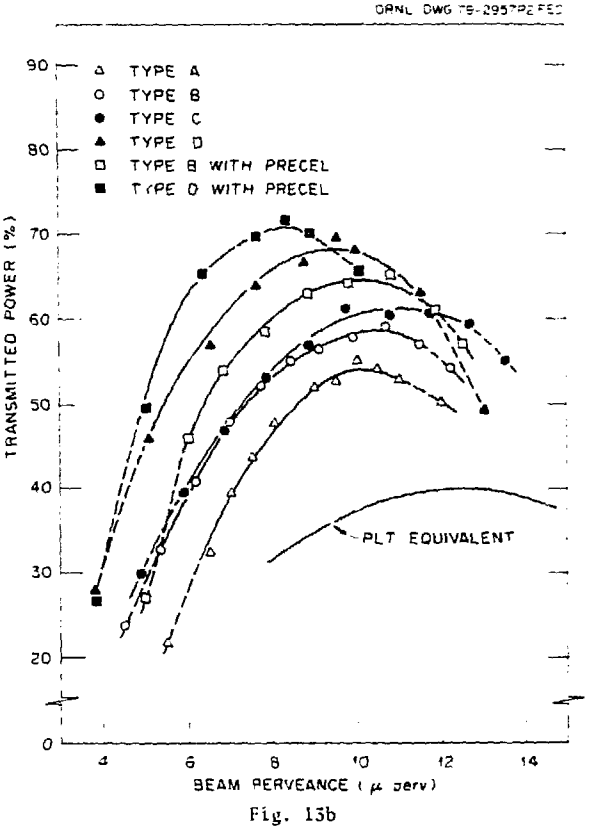

Fig. 13b

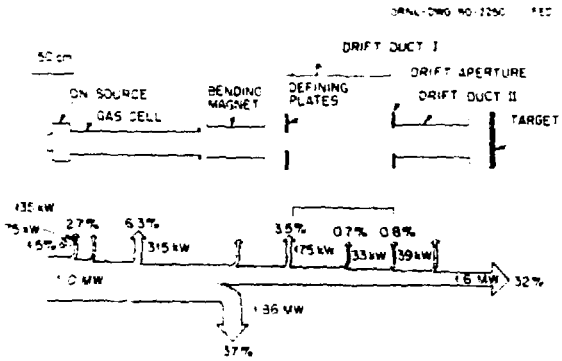

Fig. 14

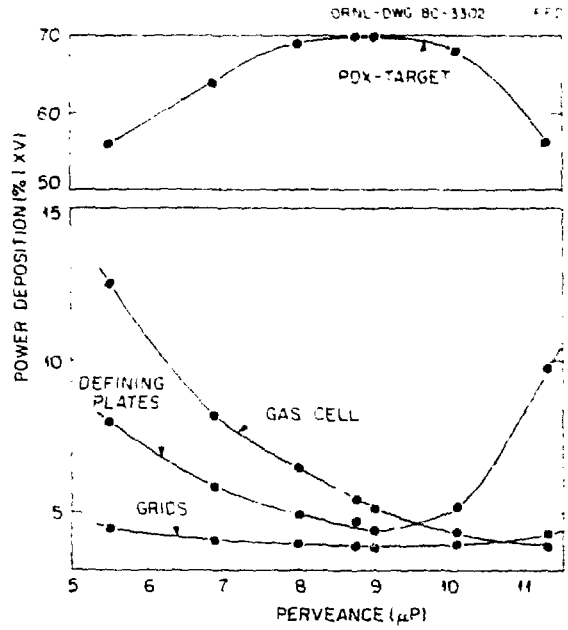

Fig. 16

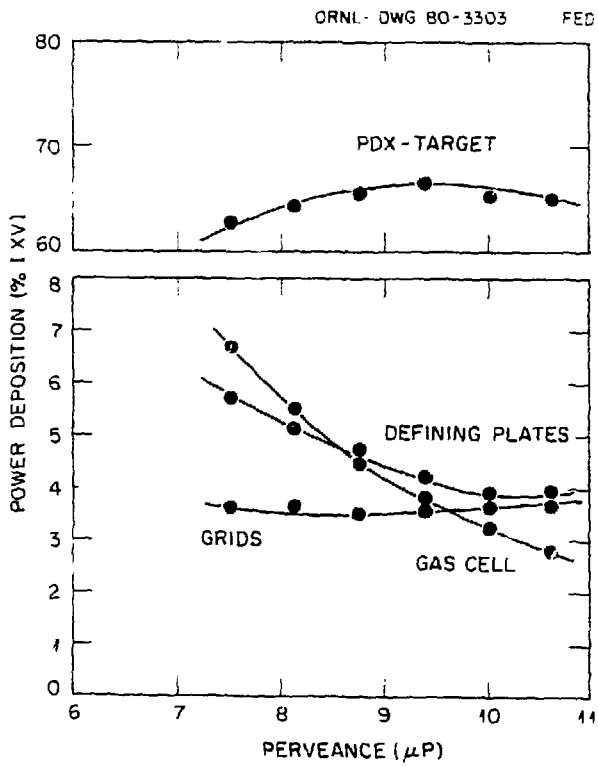

Fig. 15

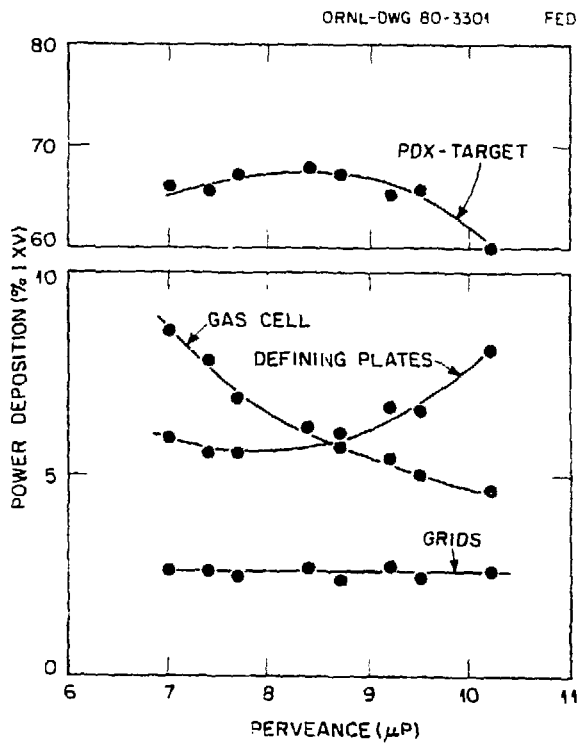

Fig. 17

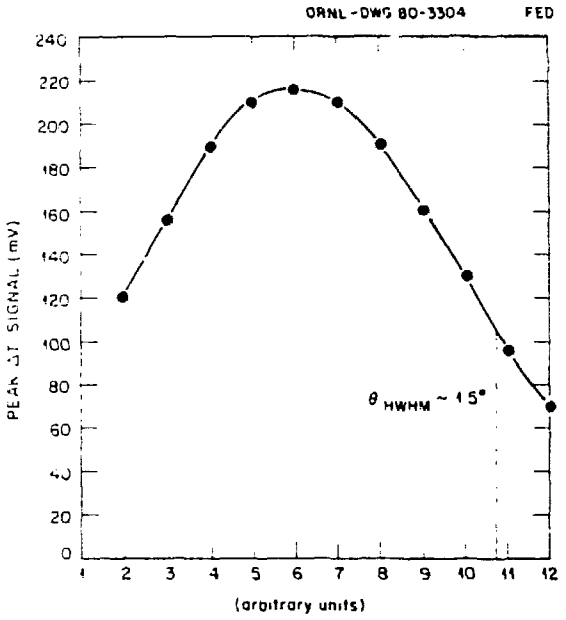

Fig. 18

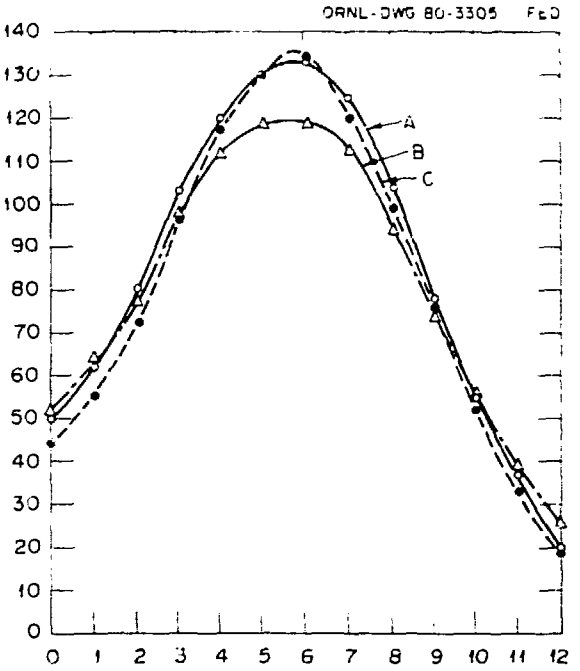

Fig. 19

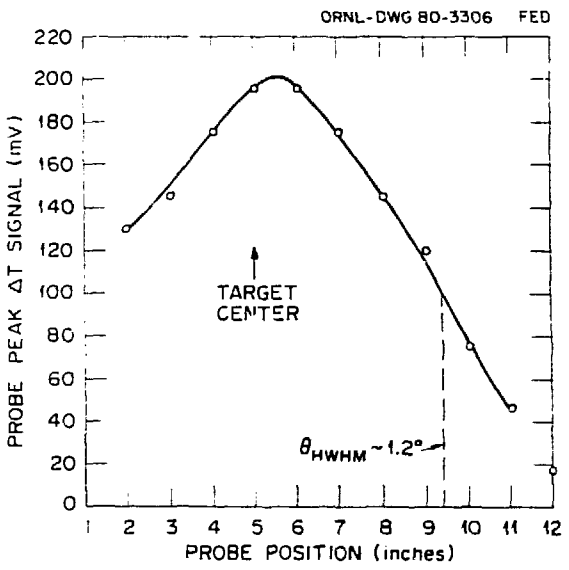

Fig. 20

Fig. 21

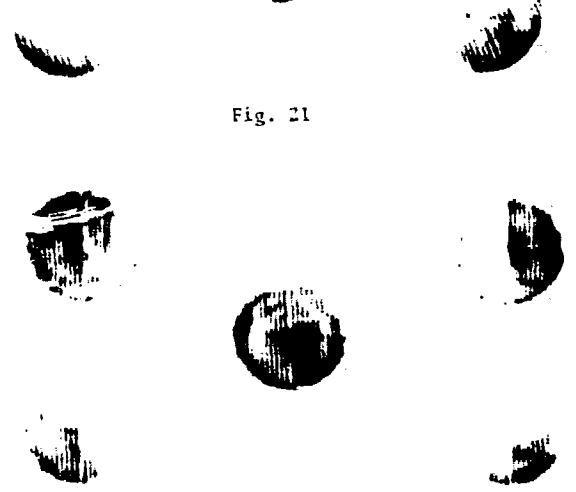

Fig. 22

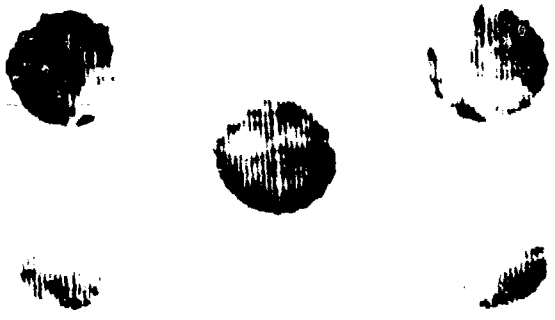

Fig. 23

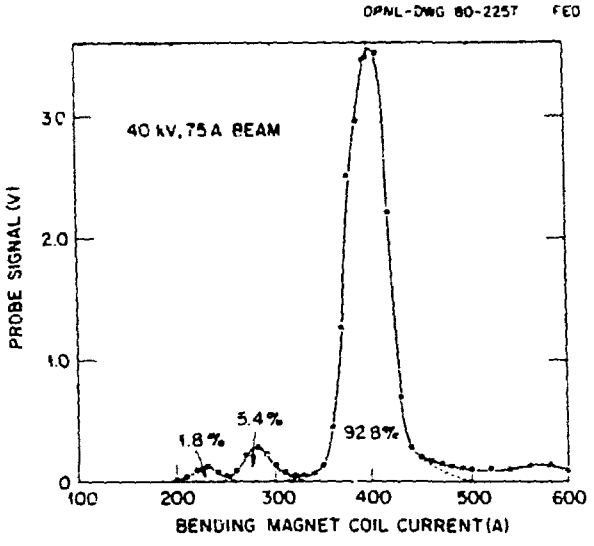

Fig. 26

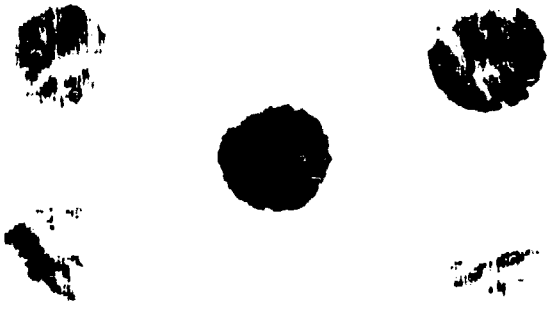

Fig. 24

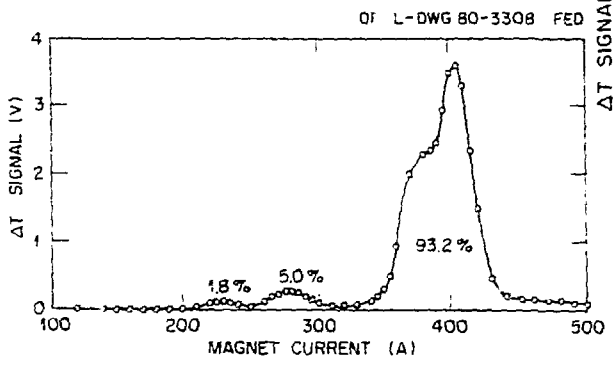

Fig. 25

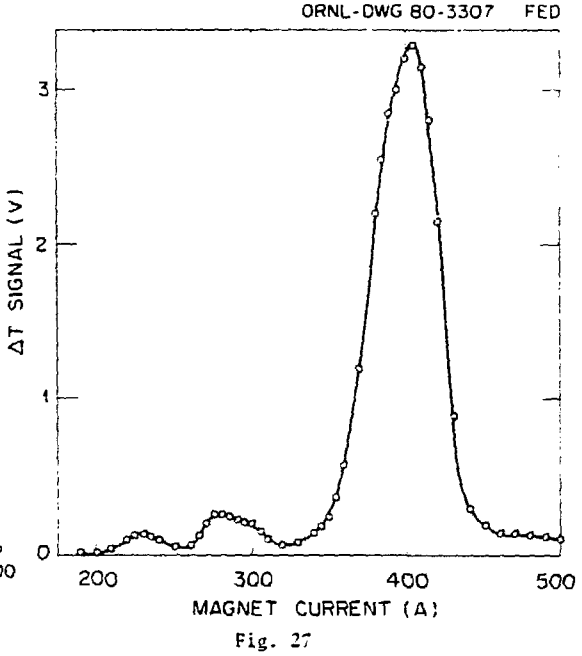

Fig. 27

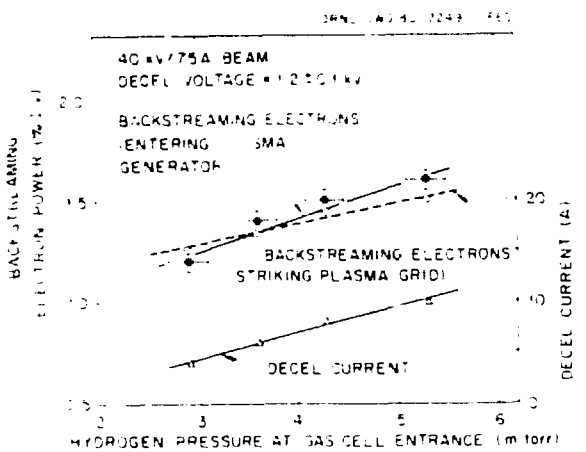

Fig. 28

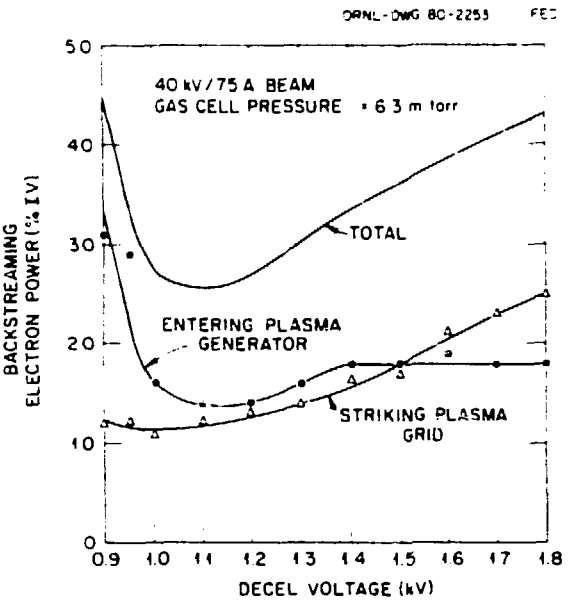

Fig. 29

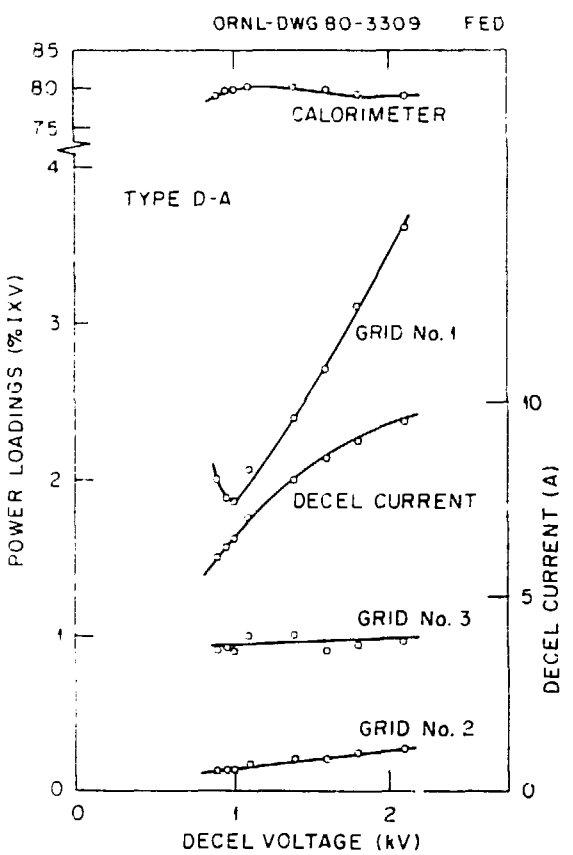

Fig. 30

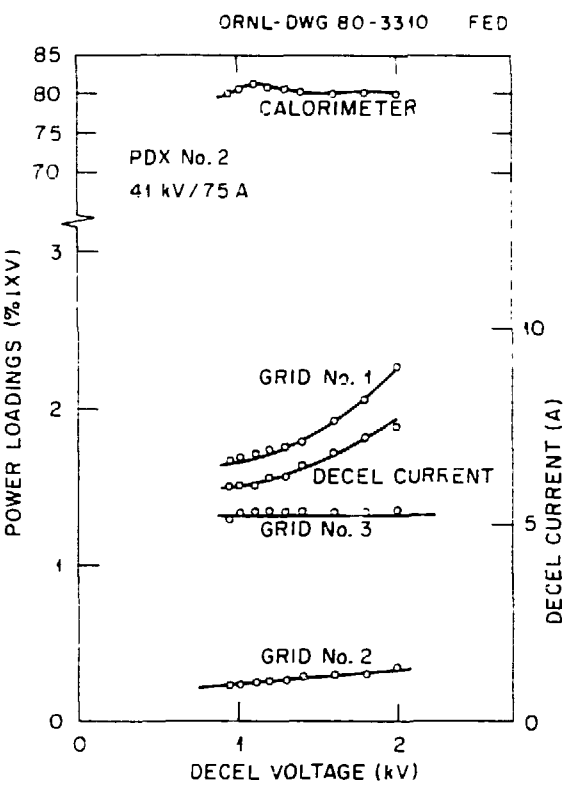

Fig. 31

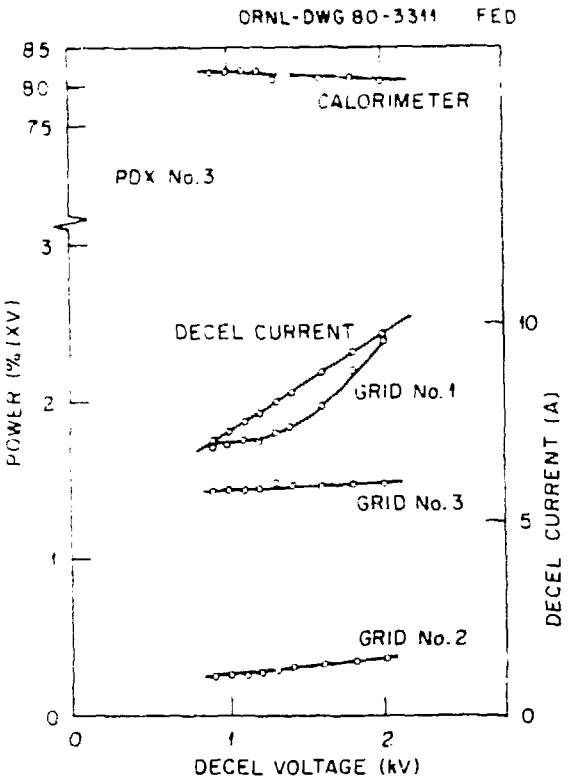

Fig. 32

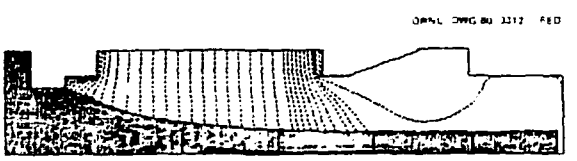

Fig. 33

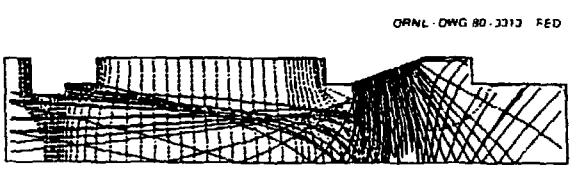

Fig. 34

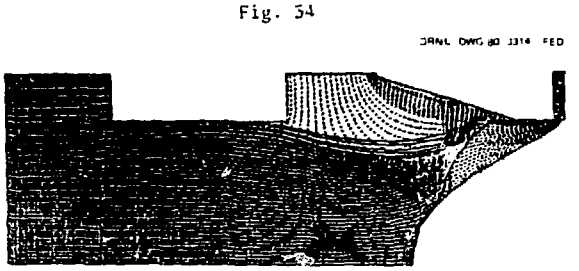

Fig. 35

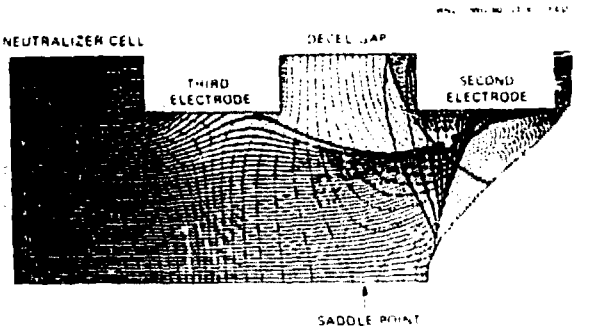

Fig. 36

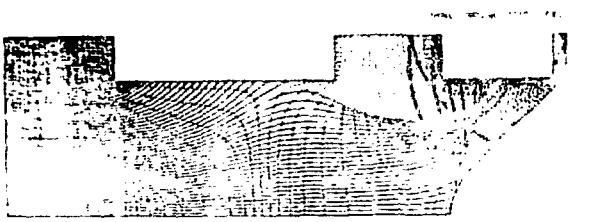

Fig. 37

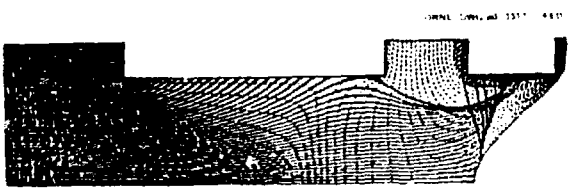

Fig. 38

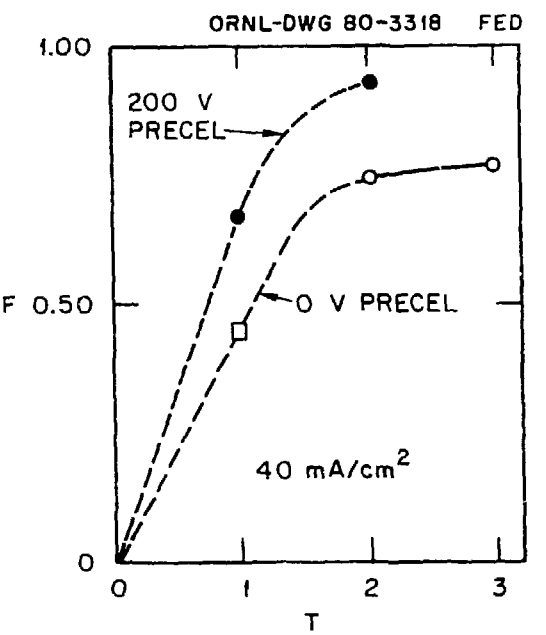

Fig. 39

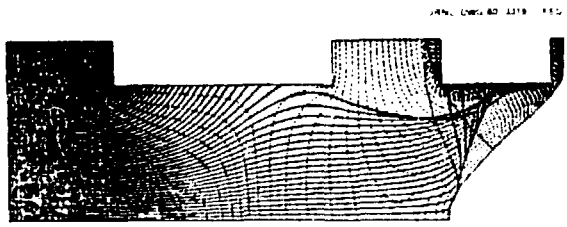

Fig. 40

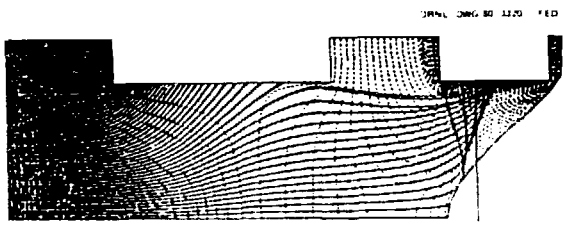

Fig. 41

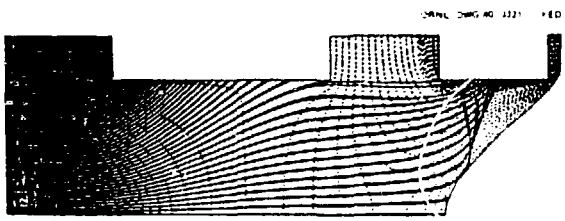

Fig. 42

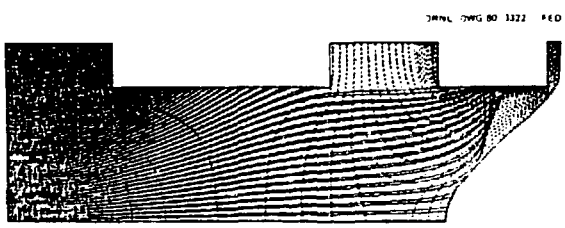

Fig. 43

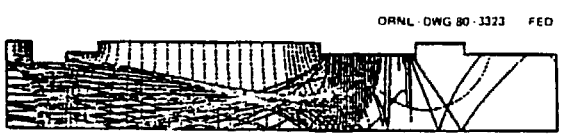

Fig. 44

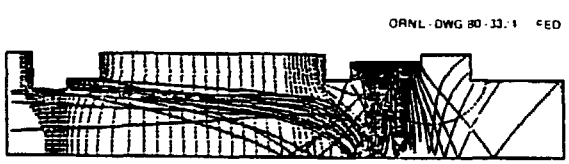

Fig. 45

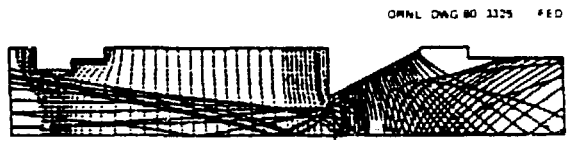

Fig. 46

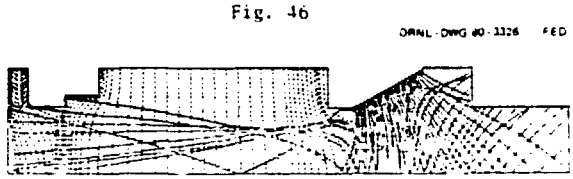

Fig. 47

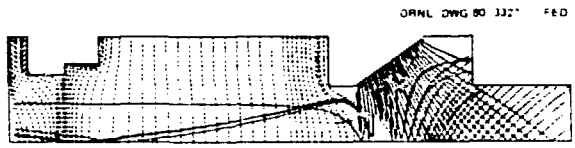

Fig. 48

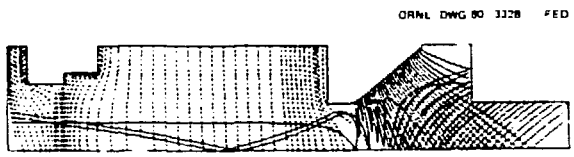

Fig. 49

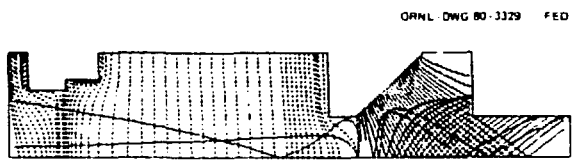

Fig. 50

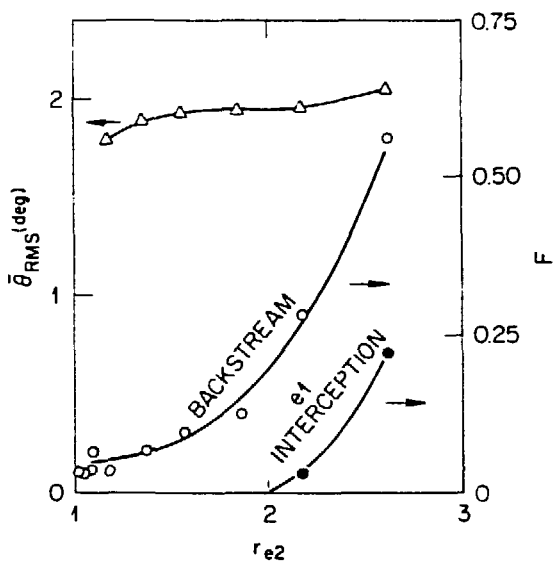

Fig. 51

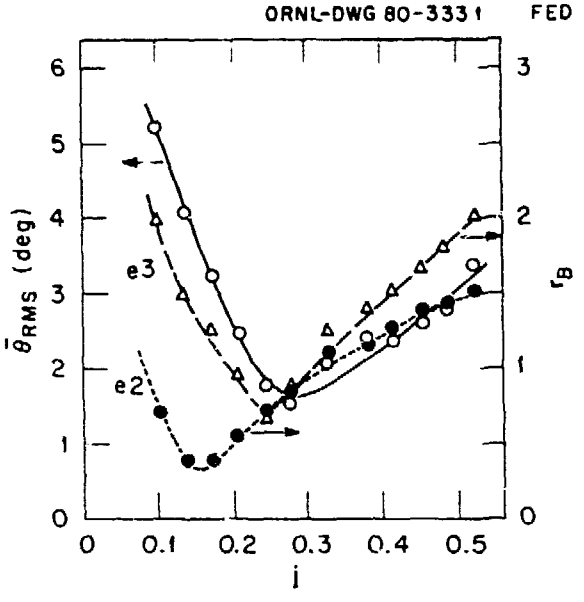

Fig. 52

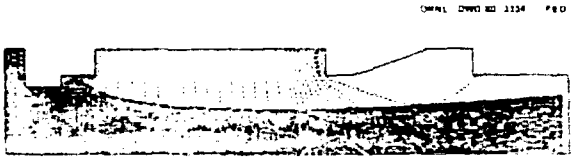

Fig. 55

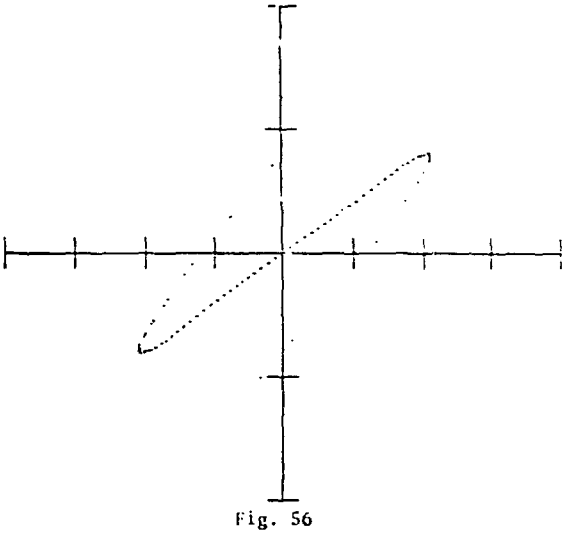

Fig. 56

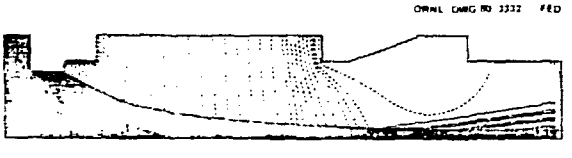

Fig. 53

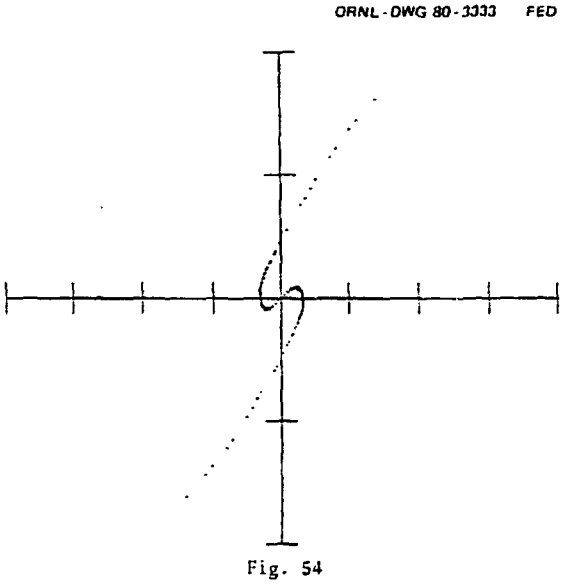

Fig. 54

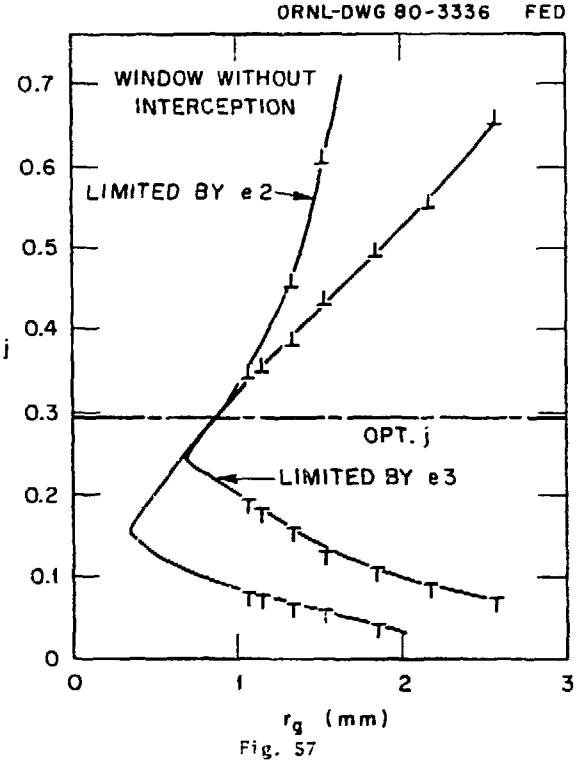

Fig. 57

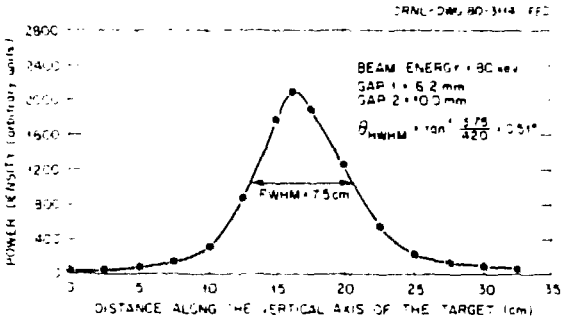

Fig. 58

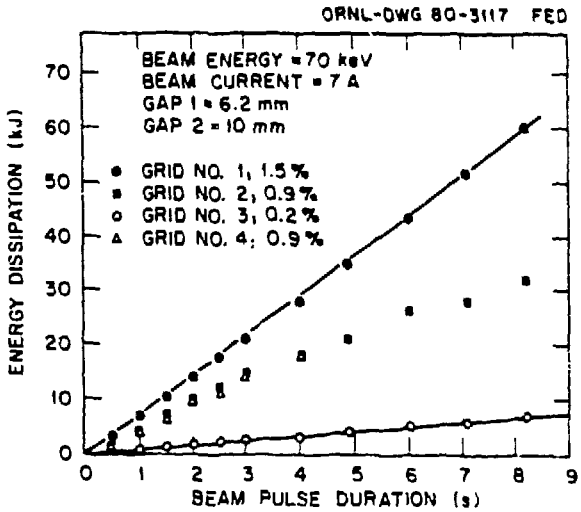

Fig. 60

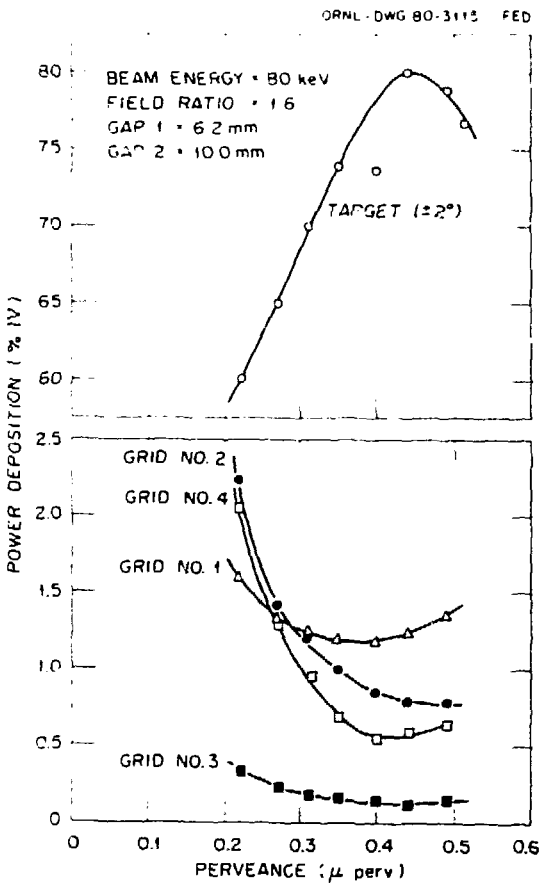

Fig. 59

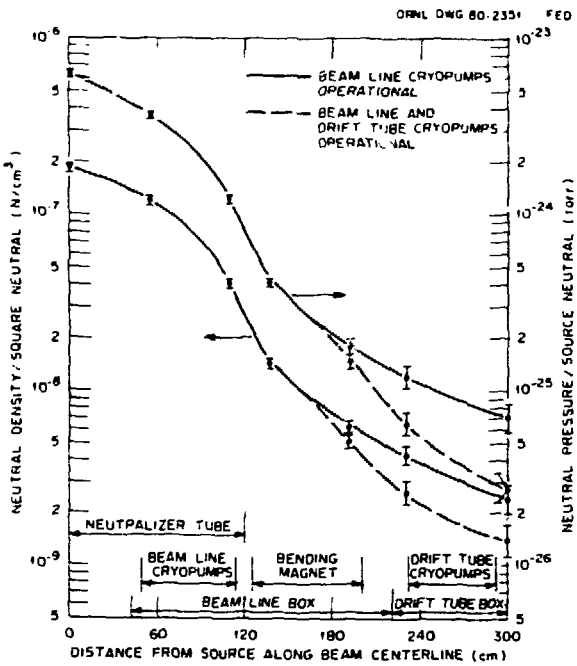

Fig. 61

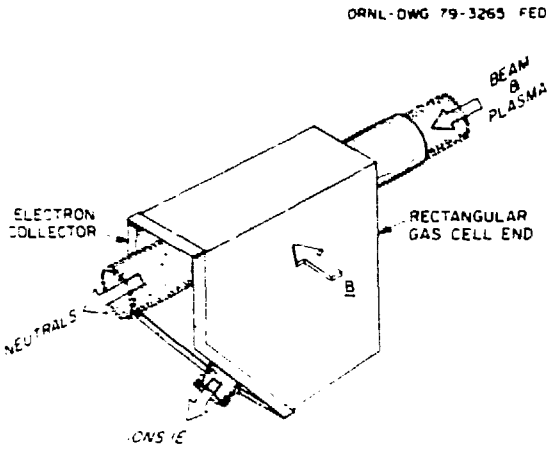

Fig. 62

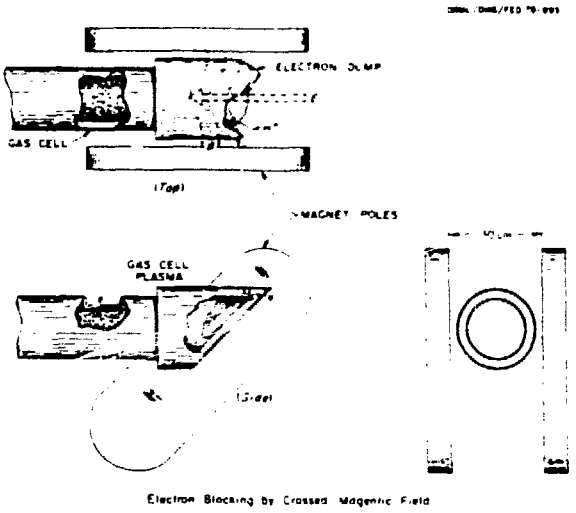

Fig. 64

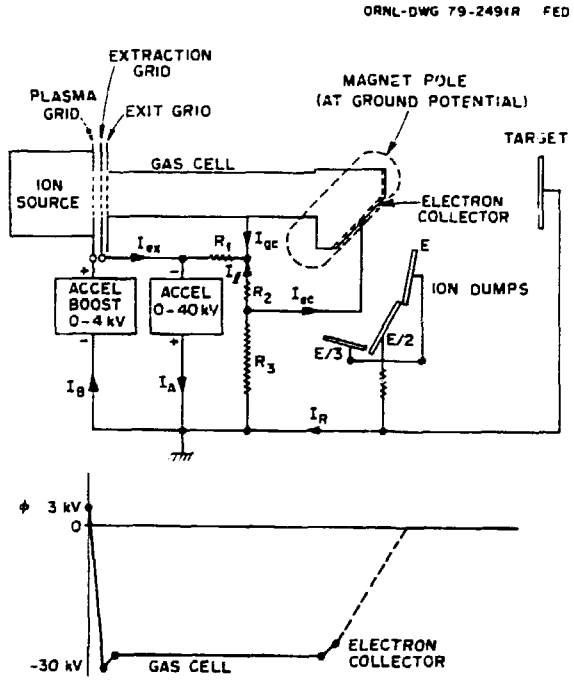

Fig. 63

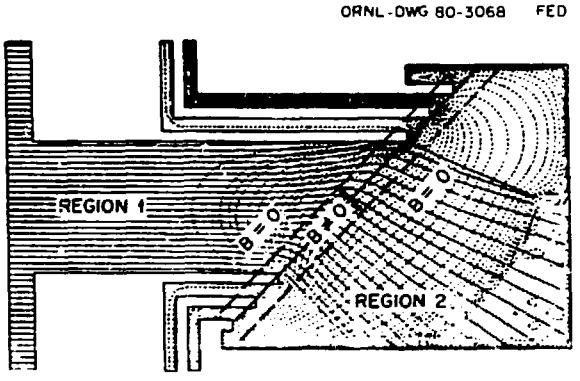

Fig. 65

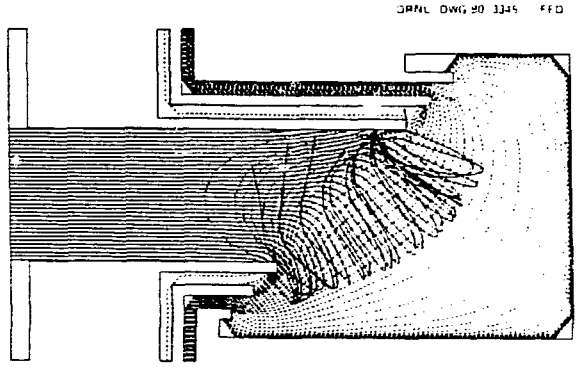

Fig. 66

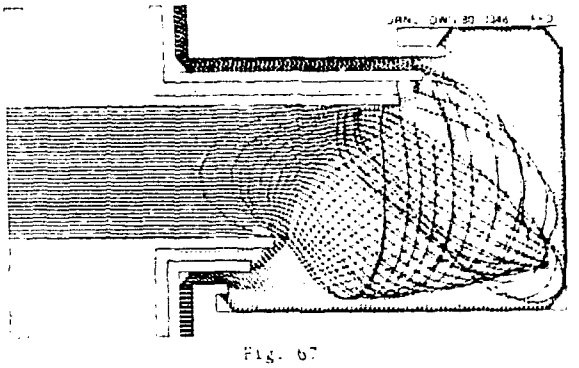

Fig. 67

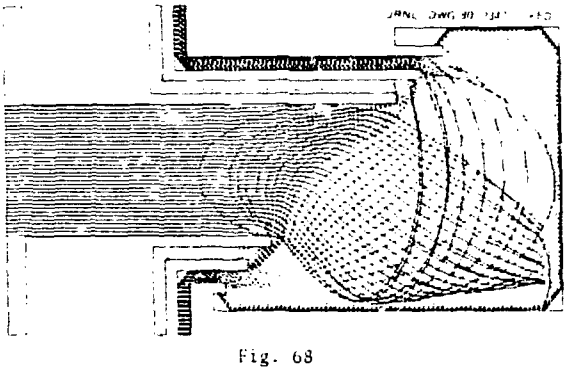

Fig. 68

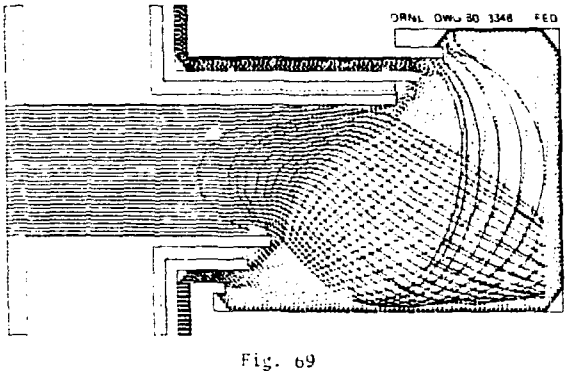

Fig. 69

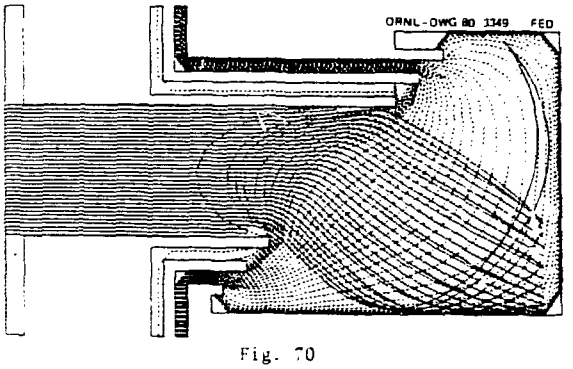

Fig. 70

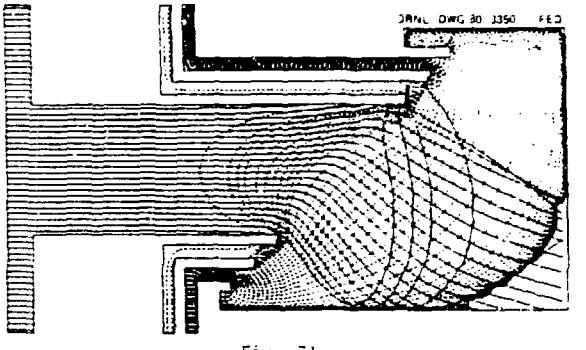

Fig. 71

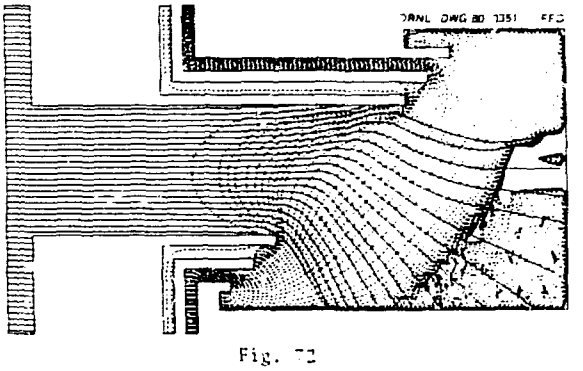

Fig. 72

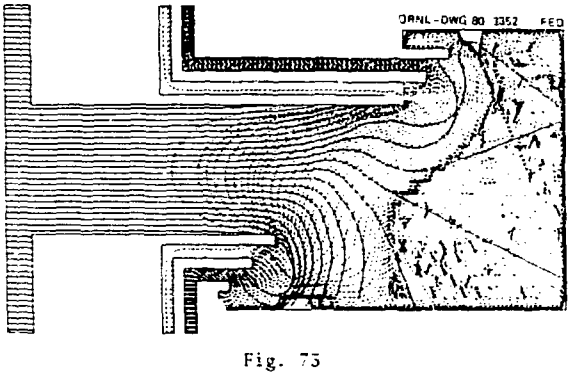

Fig. 73

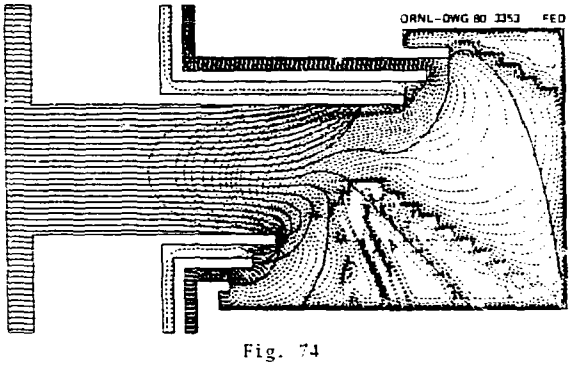

Fig. 74

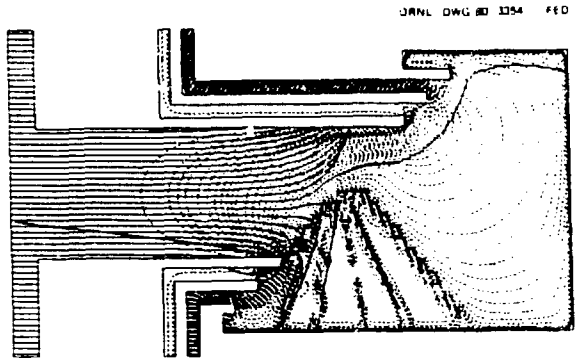

Fig. 75

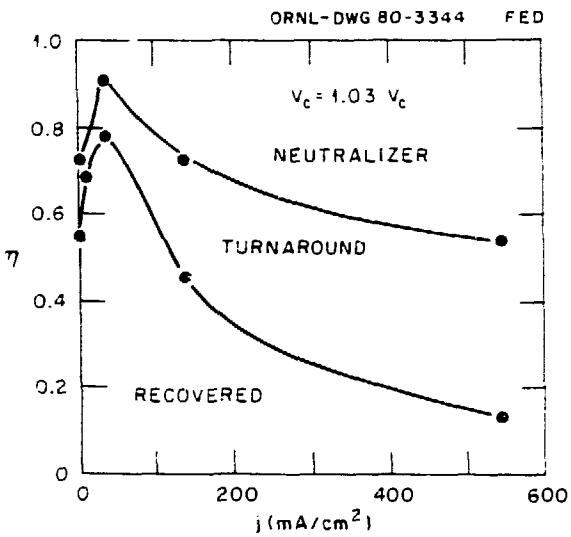

Fig. 76

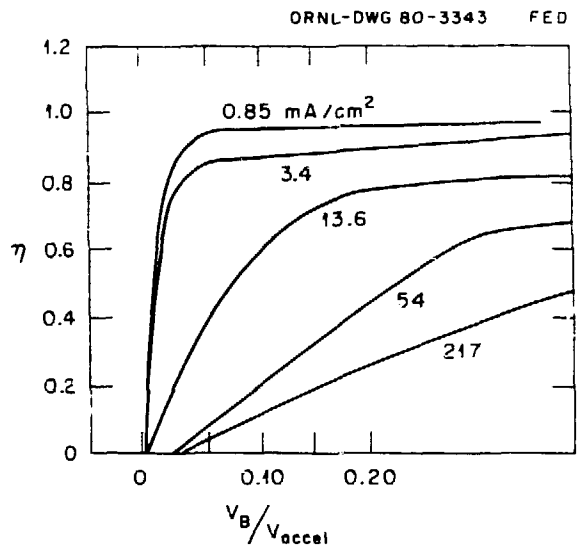

Fig. 77

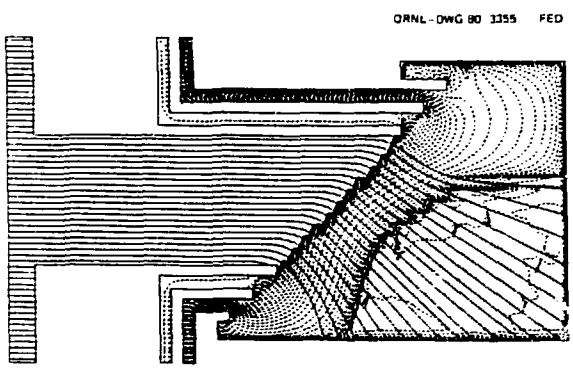

Fig. 78

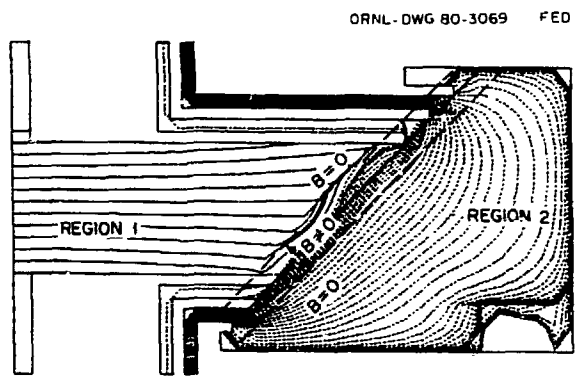

Fig. 79